OOMOLDIC POROSITY IN A MARINE REALM? A CASE STUDY FROM THE PERMIAN BASIN'S HAPPY SPRABERRY FIELD, TEXAS

A Thesis

by

AHMAD ALBADER

Submitted to the Office of Graduate and Professional Studies of
Texas A&M University
in partial fulfillment of the requirements for the degree of

MASTER OF SCIENCE

Chair of Committee, Juan Carlos Laya Pereira
Committee Members, Michael Pope
Ruud Weijermars
Head of Department, Michael Pope

May 2019

Major Subject: Geology

ABSTRACT

Due to the complex nature and importance of porosity in carbonate systems, it has been extensively studied and characterized. Many porosity types and textures have been strongly associated with certain chemical and physical conditions that they became cliché indicators of those conditions. Such associations exist for moldic and oomoldic porosity in carbonate rocks. The selective dissolution of metastable (Aragonitic or HMC) allochems has been all but accepted to indicate diagenesis by fresh waters. In this study, oomoldic porosity in the Permian Happy Spraberry Field reservoir is closely examined, in an effort to decipher the conditions that led to its creation. It is suggested that oomolds were created in a marine phreatic to shallow burial environment, with no influence whatsoever of meteoric/fresh waters.

In order to accurately characterize the conditions that led to the creation of oomolds, cement types were characterized and ranked using optical microscopy and SEM, bulk rock minerology by XRD, $\delta^{18}O$ and $\delta^{13}C$ isotope analysis, and trace element analysis by laser ablation on select samples that represent the oomoldic-rich reservoir unit of the Happy Spraberry Field Reservoir. Cements identified were mostly equant blocky LMC cements filling in primary pore spaces between ooid and bioclast molds, and some bladed isopachous LMC cements. These cements have been interpreted to be precipitated as early initial-stage cementation, and synchronous to the dissolution of the aragonitic ooids. The prominent equant LMC cement texture mimics textures associated with meteoric water diagenesis, however, further analysis proves otherwise. The LMC cements have $\delta^{18}O$ (VPDB) ratios that range between -2‰ and -3.5‰, and $\delta^{13}C$ (VPDB) ratios that range between 4‰ and 5‰. These values conform with typical low latitude Permian marine carbonate values, and further signify diagenesis within a

marine water realm. Trace element analysis of those early cements show slightly elevated Sr content, and low Fe and Mn, which is typical of marine water chemistry. Although oomolds and equant blocky cement textures are typically associated with meteoric water diagenesis, it is believed that marine waters can mimic and produce similar, if not identical textures. To explain this process, we suggest that the dissolution of aragonite ooids and precipitation of early cements to have occurred below the aragonite lysocline.

CONTRIBUTORS AND FUNDING SOURCES

Contributors

This work was supported by a thesis committee consisting of Professor Juan Carlos Laya (advisor) and Michael Pope of the Department of Geology and Geophysics and Professor Ruud Weijermars of the Department of Petroleum Engineering.

All work for the thesis was completed by the student, under the advisement of Professor Juan Carlos Laya of the Department of Geology and Geophysics.

Funding Sources

Graduate study was supported by a scholarship from Kuwait Petroleum Corporation. Its contents are solely the responsibility of the author and do not necessarily represent the official views of the Kuwait Petroleum Corporation

TABLE OF CONTENTS

LIST OF FIGURES

LIST OF TABLES

1. INTRODUCTION

Oomolds are pore spaces created from the selective dissolution of ooid grains, and where the resultant pore spaces preserve the shape of the dissolved ooids (Choquette and Pray, 1970). The ooids' susceptibility to dissolution is attributed to their minerology, where most ooids are deposited as metastable aragonite and/or high-Mg calcite (Heydari et al., 1993). The dissolution of metastable, aragonitic ooids is traditionally regarded as a near-surface freshwater diagenetic process (James and Choquette, 1984; Moore, 1989; Sun, 1992). The most interpreted mechanisms for aragonite dissolution include fresh water dissolution as a result of exposure or ground water flow, mixing-zone phreatic water dissolution, microbially induced dissolution, and deep burial dissolution by hydrothermal fluids (Frank et al., 2011; James and Choquette, 1984; Swart, 2015). The selective dissolution of aragonite is especially common in oolite beds (ooid-rich limestone). Consequently, almost all moldic ooid porosity, whether recent or ancient, was explained by using one of these models. Oolites are important because they often are used to reconstruct past environments, especially since they are very common throughout the geological record, from the Precambrian to the present-day (Mariotti et al., 2015). These types of deposits also form some of the best carbonate hydrocarbon reservoirs and comprise a large share of global carbonate reservoirs (Lehrmann et al., 2012). Hence, a thorough understanding of the moldic ooid porosity's genesis, storage capacity, and producibility is of extreme importance in order to efficiently exploit these resources.

The processes and mechanisms that induce aragonitic ooid dissolution are almost exclusively associated with meteoric water influence. Although it is a viable mechanism, and probably the most common, other possibilities should be explored, especially if signals of

meteoric influence are vague or absent. To understand these processes, and since they share a close genetic relationship, cements surrounding ooid molds are key to interpreting their diagenetic history. Oomolds and their associated cements in the Happy Spraberry Field, Texas are examined in this study to determine the environments and processes that induced the formation of ooids, their dissolution, and precipitation of surrounding cements.

Although the prominent porosity type (oomoldic) and cement minerology (LMC) typically are interpreted as resulting from carbonate interaction with meteoric waters, some features in the Happy Spraberry oolitic succession point towards other possible origins. We hypothesize that the processes of dissolution of ooids and precipitation of LMC cements occurred within the marine phreatic realm. One possible mechanism that causes aragonitic ooid dissolution in marine waters is that the deposits were in water undersaturated with respect to aragonite. It was suggested that dissolution and dolomitization of aragonite and calcite in Enewetak Atoll was caused by invading cold undersaturated marine waters (Saller, 1986). Alternatively, oomoldic porosity and LMC cements of periplatform sediments in the Bahamas formed in saturated shallow waters above the aragonite compensation depth (ACD), defined as the depth below which aragonite is completely dissolved from sediments (Milliman et al., 1999), to be in isotopic equilibrium with marine waters (Melim et al., 2002; Melim et al., 1995). Although the Happy Field was deposited on a gentle slope environment, it was interpreted from seismic sections that its deposition occurred 4 miles basinward of the eastern shelf of the Midland Basin (Gentry, 2005). This suggests these aragonitic ooid deposits were re-worked to a depth of possibly several hundreds of meters, and closer to colder basinal waters undersaturated with respect to aragonite within the aragonite lysocline, or possibly below the ACD.

Ooid molds in the Happy Spraberry field show characteristics typical of molds created from meteoric water dissolution of aragonite, in the form of selective dissolution of ooids, and the precipitation of equant calcite cement (James and Choquette, 1984; Longman, 1980). In some cases, the presence of molds alone drives the interpretation of meteoric water dissolution. However, signs of exposure or meteoric water influence, in the form of caliche crusts, rhizoliths, and breccias, or meteoric water cement textures, such as stalactitic or meniscus cements do not occur in the succession. In fact, textures such as isopachous cements and micrite envelopes are common in these rocks, suggesting precipitation of these cements in a marine environment (Andrieu et al., 2018; Reid and Macintyre, 1998).

This study tests the hypothesis that the dissolution of aragonite and precipitation of LMC cements in the Happy Spraberry Field occurred in marine waters. Through examining early cement textures, minerology, and C and O stable isotope values, it is the aim to establish a mechanism/model that explains oomoldic porosity creation in the slope deposits as observed in the Happy Spraberry Field, and explore the implications of aragonite dissolution in different environments.

1.1. Genesis and evolution of terminology

Ooid rich limestone has been described for centuries. The first documented observation of ooid rich limestone was made by Pliny during the first century A.D. observing rocks, he named Hammites, that looked similar to the spawn of fish, and classing them as precious rocks (Burne et al., 2012; Dahanayake et al., 1985). The first microscopic observation of oolites came as early as 1664 by Robert Hooke, who described rocks from Kettering Northamptonshire as being made

up of small structures that appear like the cob or ovary of a herring (Brown, 1914; Burne et al., 2012). The predecessor to the term 'oolite' was first coined by Volkmann in 1720 referring to the rock as *oolithos*, which is the Greek translation of the German *rogenstein*, meaning egg-stone (Burne et al., 2012). Perhaps the first English use of the word 'oolite' was introduced by Hutton in 1788 (Burne et al., 2012), however the first proper English definition of the word 'oolite' came in 1855 by Sir Charles Lyell (Richter, 1983), in which he states,

> *"The variety of limestone called 'oolite' is composed of numerous small egg-like grains, resembling the roe of a fish, each of which has usually a small fragment of sand as a nucleus, around which concentric layers of calcareous matter have accumulated"* (Lyell, 1855).

Then in 1908, a further distinction was made between the oolite rock, and the grains that make up the rock, in which Kalkowsky named 'ooids' (Kalkowsky, 1908; Richter, 1983; Simone, 1980). However, as his publication was in German, most English publications continued with the use of 'ooliths' to describe the grains that make up oolitic rocks. In 1945, a proposal was suggested to name the grains as 'ooids' in preference to 'ooliths' (Cloud et al., 1945; DeFord and Waldschmidt, 1946). Yet the term 'ooid' was seldom used until Teichert's proposal, or plea, to resurrect Kalkowsky's term 'ooid' for the component particles of an oolite and to avoid the ambiguous term 'oolith'. (Burne et al., 2012; Teichert, 1970).

By this time, oolitic rocks and their properties were fairly well studied, and theories began to rise discussing the origins of oolites, textures, and diagenetic features. Since the earlier days, for example, it was suggested that the dissolution of ooids was a result of their original mineralogy, alluding to aragonite for being the more soluble phase of carbonate (Sorby, 1879). The voids created by dissolved ooid grains were referred to as solution cavities, and casts. Two later terms, oolicastic and oocastic pores, were suggested following McQueen's (1931)

description of voids in dolomite which he called dolocasts (Cole, 1942; Crowley and Hendricks, 1945). Finally in 1945, the term 'oomoldic' was introduced and defined as a subspherical hole or mold of a previously oolitic or oocastic chert where the original ooids or their replacement have been removed (Cloud et al., 1945). Although similar to previous definitions, Choquette and Pray (1970) went on to define moldic and oomoldic porosity as "a pore formed by the selective removal, normally by solution, of a former individual constituent of the sediment or rock such as a shell or oolith", and added, "if the identity of the mold is known, it can be added to the porosity term, a long-established practice with terms like 'oomold' or 'oomoldic' and 'dolomold' or 'dolomoldic'." The terms mold, moldic, and oomoldic seem to be the most accepted and hence the most ubiquitous in geological literature today.

1.2. Porosity in oolitic facies

Porosity types within oolitic sediments generally are sub-divided into two types: primary (depositional) and secondary (diagenetic) porosities. Primary porosity includes interparticle pore space, whereas secondary porosity includes intercrystalline, moldic, vugs, channels, fractures, and caverns (Choquette and Pray, 1970). Moldic porosity is created from the selective dissolution of metastable allochems, and the resultant pore space preserves the shape, or mold, of the dissolved material (Choquette and Pray, 1970). Moldic porosity that is a result of the dissolution of ooid grains is referred to as oomoldic porosity (Tucker and Wright, 1990).

Aragonite and calcite ooids behave differently with regard to dissolution and cementation. Aragonite is the most soluble carbonate phase, and is prone to early dissolution, followed by high-Mg calcite and low-Mg calcite respectively. However, the majority of observations indicate that oomoldic porosity suggests an aragonite precursor, whereas high-Mg calcite ooids

transform to low-Mg calcite ooids while preserving their original crystal morphology (Heydari et al., 1993; Sandberg, 1985).

1.3. Cementation

Cementation within oolitic rocks is a significant element that preserves relict ooids. We think that cementation stages are intimately related to the origin and evolution of the oomoldic porosity. These cements are the witnesses of dissolution, and record evidence of the nature of the diagenetic waters that caused dissolution in their texture and minerology. Early cementation within oolite rocks can be grouped into two main environments: 1) meteoric/freshwater and 2) marine. Fresh water cementation typically is low Mg-calcite (LMC) and can occur in two main zones: the vadose zone above the water table, and the phreatic zone below the water table (James and Choquette, 1984; Longman, 1980). Typical vadose zone cements include meniscus, pendant, or stalactitic cements, and minor equant calcite, whereas phreatic zone textures mainly are equant calcite cements, drusy cements, and syntaxial overgrowths (James and Choquette, 1984; Longman, 1980). Marine cementation usually occurs from the seafloor to shallow burial, and typically is characterized by aragonite and high Mg-calcite (HMC) precipitation in the form of aragonite needles, isopachous fibrous and bladed cements, botryoidal cements, radiaxial, and micritic envelopes and fillings (Kerans et al., 1986; Longman, 1980). Also, cement minerology is influenced by global seawater geochemistry and climate, in which periods of greenhouse climate feature dominant LMC precipitation, and periods of icehouse climate feature dominant aragonite and HMC precipitation (Palmer and Wilson, 2004; Stanley and Hardie, 1998).

2. BACKGROUND

2.1. Study area and geological setting

The Permian Basin, located in west Texas and southern New Mexico, covers an area of ~300,000 km^2 (Mazzullo, 1995). Its tectonic and depositional history is sub-divided into three main stages (Sarg et al., 1999; Ward et al., 1986). The first stage spans the Late Cambrian through the Early Mississippian and marks the development of a passive margin along the southern margin of the North American Plate (Sarg et al., 1999). This period witnessed vast deposition of shallow marine Upper Cambrian to Upper Devonian carbonate, and rare siliciclastic rocks in the Tobosa Basin, the predecessor to the Permian Basin (Mazzullo, 1995). The second stage marks the collision of the North American Plate with Gondwana during the Mississippian through the Early Permian. This collision produced the Ouachita-Marathon orogenic belt and deformed the Tobosa basin into several coeval foreland basins (Sarg et al., 1999). This event created the present-day configuration of the Permian Basin with several basins (e.g., Delaware, Midland, Val Verde) separated by structural highs (e.g., Central Basin Platform, Diablo Platform, Eastern Shelf; Mazzullo, 1995; Sarg et al., 1999). During the Early Pennsylvanian, thick siliciclastic sedimentation dominated as a result of the intense tectonic activity (Ward et al., 1986; Yang and Dorobek, 1995). But as the region continued to drift to warmer equatorial locations, platform growth was accentuated with carbonate deposition contributing more to the overall accumulation of sediments (Mazzullo, 1995). The third stage, in the Early to Late Permian, marks a period of structural stability and tectonic quiescence (Atchley et al., 1999). In the Mid-to-Late Permian, a shift towards more arid conditions all but terminated carbonate production on the Central Basin Platform, Midland Basin, and Eastern Shelf, and

resulted in the deposition and accumulation of thick evaporite and siliciclastic sequences (Mazzullo, 1995; Ward et al., 1986).

2.2. Happy Spraberry Field

The proposed research is conducted in the Happy Spraberry Field located in Garza County in northwest Texas (figure 1). This field was first discovered in 1988 by Bennet Petroleum during the re-completion of a previously abandoned Ellenberger well (Clayton, 2011). Although called the Happy Spraberry Field, it was later correlated to the Early Permian Lower Clear Fork Formation, which is time equivalent to the basinal Dean Sandstone Formation in the Midland Basin (Layman, 2004).

The main reservoir zone in the Happy Spraberry Field is composed of ooid-skeletal grainstone and packstone beds (figure 2,3), ranging in thickness from 15-50 ft. in most of the wells, and at a depth of about 4950 ft. The main reservoir zone is formed of mostly originally aragonitic ooids, sometimes reaching up to 75% of the rock volume, as well as brachiopods, bryozoans, ostracods, and crinoids (Mazingue-Desailly, 2004). However, most of the ooids and allochems are partly or completely dissolved. Accordingly, oomoldic porosity is the most prominent porosity type within the reservoir.

The reservoir interval at the Happy Spraberry Field is interpreted to be Leonardian (figure 4; Ahr and Hammel, 1999). However, accurate stratigraphic correlations between units on the Eastern Shelf and the Midland Basin often are difficult because of the 2000 feet vertical structural relief separating the areas, leading to complicated and widespread facies changes

between coeval beds (Handford, 1981). In fact, two different interpretations based on seismic data were proposed relating to the age of the Happy Spraberry reservoir. Some interpreted its age to be Upper Leonardian, and part of the Upper Clear Fork and its basinal equivalent the Upper Spraberry Formations (e.g., Clayton, 2011; Hammel, 1996); others interpreted it to be part of the Lower Clear Fork Formation (e.g., Gentry, 2005; Layman, 2004).

The Happy Spraberry Field was well studied multiple times because of the availability of data. Various theses and papers were published about this reservoir (e.g., Ahr and Hammel, 1999; Clayton, 2011; Layman, 2004; Mazingue-Desailly, 2004). Although specifics like lithology and diagenetic overprints are well understood, contradicting views arose regarding the depositional environment of the reservoir rock. One view hypothesizes that deposition occurred in a shallow upper slope environment (Ahr and Hammel, 1999), whereas others suggest that these sediments were re-worked and deposited in deeper slope environments (Gentry, 2005; Mazzullo, 1995). What is still unclear is the source of diagenetic waters that caused the early dissolution of aragonite and subsequent precipitation of LMC cements.

3. DATA AND METHODOLOGY

Nine downhole cores from the central part of Happy Spraberry field are available in Texas A&M University's core repository. Core descriptions were available from previous work and were utilized, along with additional description, to identify intervals of interest *i.e.* that showed ooid dominated facies within the reservoir section of the core. Initially 59 thin sections were available for various intervals from 5 different wells, and 102 additional thin sections were cut from intervals of oolitic grainstone, packstone and wackestone facies from all 9 wells. Slides were impregnated with blue epoxy to highlight porosity and later stained with Alizarin red to differentiate calcite from dolomite.

Various methods were utilized to adequately address the proposed hypothesis, that oomoldic porosity was created in a marine environment. First, polished thin sections were analyzed petrographically to characterize porosity, cement types, and paragenesis, and identify microfacies using the Olympus BX53MTRF petrographic microscope. Additionally pore, grain and cement analyses were performed using the Phenom World Phenom XL scanning electron microscope.

Oxygen and carbon stable isotope analysis ($\delta^{18}O$ and $\delta^{13}C$) of grains and cements was performed using the Thermo Scientific Kiel IV Carbonate Device at the Stable Isotope Geosciences Facility (SIGF) at Texas A&M University to identify the sources and characteristics of the diagenetic events. Samples were collected using a micro-tip dental pick and collected in clean and dried vials. At least 20 micrograms of carbonate material were needed for each sample. A total of 29 coupled $\delta^{18}O$ and $\delta^{13}C$ measurements were performed. All results are

reported as delta Carbon or Oxygen ($\delta^{13}C$ and $\delta^{18}O$) in per mil deviations from the Vienna Pee Dee Belemnite standard (‰VPDB), where $\delta^{13}C$ and $\delta^{18}O = (R_{sample} - R_{standard}) / (R_{standard}) \times 1000$, and R_{sample} and $R_{standard}$ represent the $^{13}C/^{12}C$ and $^{18}O/^{16}O$ molar ratios of the sample and standard respectively. Analysis precision was reported at ±0.04‰ for $\delta^{13}C$ and ±0.06‰ for $\delta^{18}O$.

LMC shells are most resistant to diagenetic alteration, and most representative of the primary geochemical signal. Therefore, the sampling of unaltered brachiopod shells was necessary in order to establish a baseline relative to which the effects of diagenesis can be evaluated. Before sampling, the brachiopod shells were first examined by optical microscopy, and elemental analysis was performed using the Phenom XL scanning electron microscope (SEM) in order to confirm the preservation state of the shells and the LMC minerology. Only shells that showed lamellar or foliated microtextures typical of well-preserved brachiopod shells were sampled (Korte et al., 2008). Shells that showed traces of post-depositional dissolution and/or recrystallization were neglected.

Six samples from 4 different wells had their trace elements analyzed by the Analyte193 Ultra-short Pulse Excimer Laser Ablation. A total of 223 points were analyzed for 4 different cement/grain types. The points mainly represent the 1) blocky equant cements, 2) isopachous cements, 3) micritized ooids, and 4) brachiopod shells. XRD analysis also was performed on 22 rock samples from 7 different wells using a Rigaku Miniflex X-ray Diffractometer to identify bulk rock mineralogy. In addition, a scanning electron microscope, Phenom XL from Nanoscience technology, was used to examine cement textures, and perform elemental analysis on grains and cements.

4. RESULTS

4.1. Happy Spraberry facies

Five main lithofacies occur in the Happy Spraberry field. Facies were interpreted from core slabs, thin sections, and well log data. The main reservoir facies are oolitic grainstone and packstone. Rudstone and floatstone facies underlie the grainstone and packstone facies, and shaly siltstone facies overlie and underlie the carbonate succession. Facies and their descriptions are presented in table 1, and a facies type log can be seen in figure 3.

4.2. Petrographic observations of ooid facies

Petrographic analysis indicates the oolitic successions (e.g. grainstone and packstone) normally are composed of >50% ooid grains, and some fragments of crinoids, brachiopods, bryozoans, and foraminifers. The ooid grains are mostly dissolved and appear as voids 0.2-0.4 mm in diameter with a micritic envelope, whereas a small portion were either completely or partially micritized or cemented. The matrix commonly is lime-mudstone varying in abundance from almost non-existent in grainstone facies to common in floatstone facies. Five diagenetic features (figure 5), in order of most to least abundant, are: 1) blocky equant drusy calcite spar (C1), 2) micrite envelopes surrounding ooids (C2), 3) isopachous cements (C3), dolomite cement (C4), and poikilotopic cements (C5).

4.3. Minerology and geochemistry of ooid facies

4.3.1 XRD

Bulk rock XRD was analyzed on 22 rock samples. Most samples showed dominant calcite mineralogy, except for samples containing poikilotopic cement (well 19-4 4920, 4930,

and 4958), which contain anomalously high values of celestine. All samples showed dominant low Mg-calcite concentrations (<4 w.t.% Mg). Trace concentrations of quartz were detected in 9 samples, and 1 sample contained minor detectable dolomite content. There was no trace of aragonite in any of the samples. Results are summarized in table 2.

4.3.2 Stable isotopes

29 samples from 8 different wells were analyzed for $\delta^{18}O$ and $\delta^{13}C$ isotopes (figure 6). The majority of samples, 26, were of blocky equant cements (C1) and 3 samples were of unaltered brachiopod shells. $\delta^{18}O$ values ranged from -3.5 to -1.5‰, whereas $\delta^{13}C$ values ranged from 3.5 to 5‰. Brachiopod samples showed less variance, with $\delta^{18}O$ values ranging from -2.9 to -3.5‰, and $\delta^{13}C$ values of 3.9‰.

4.3.3. Trace elements

Trace elements analysis was performed to determine concentrations of Ca, Mg, Sr, Fe, Mn, and Na. A total of 223 points were analyzed for four different types of cements/grains. 119 points were of the equant blocky calcite cement, 32 were of the isopachous cements, 36 were of micritized ooids, and 36 were of brachiopod shells. Results are presented in table 3.

Mg concentrations (figure 7) are relatively low, ranging from about 2000 to 9000 ppm with few samples having concentrations larger than 9000 ppm. Brachiopod shells showed expected low Mg concentrations. A few anomalously high Mg concentrations above 15,000 ppm did occur, however they were not restricted to a specific cement type. All samples had concentrations of less than 4 w.t.% Mg content.

As illustrated in figure 8, Fe and Mn behave in a similar manner and their absolute concentrations are relatively low. It almost seems as if they are co-dependent, as Mn values increase, so do Fe values. The samples with the least spread were those of the brachiopod shells, with Fe and Mn ranging from 202-263 ppm and 4-99 ppm respectively. The cements also had similar values with mean Fe and Mn concentrations at 293 ppm and 58 ppm respectively.

Sr concentrations (figure 9), for most samples, are not very variable. Most samples from all different cement/grain types have a range from 200 ppm to 900 ppm. Only 10 points of equant blocky cements lie outside this range, with values ranging between 1000 to 2332 ppm. The average Sr concentration for all points is 605 ppm.

5. DISCUSSION

5.1. Ooid formation and deposition in marine environments

Marine ooids typically are deposited in shoreface settings of ramps, on inner platforms, and near the outer margins of platforms, within high-energy wave dominated shallow sand bars or tidal channels (Bosellini et al., 1981; Tan et al., 2012). Sand bars develop in platform margin sites in water depths ranging between 0-10 m (Harris et al., 2018; Harris et al., 2015). Ooids also occur in deep-water settings, as allochthonous shallow water deposits re-sedimented, as a result of debris flow or turbidites, in the toe-of-slope and basinal settings. In this setting, they often are poorly sorted and occur with lithoclasts and shallow-marine, platform-derived skeletal grains (Zempolich and Erba, 1999).

5.2. Questioning classical models

Dissolution of ooids, and the creation of porosity, generally occurs in response to a significant change in the chemistry of the pore fluid, such as a change in temperature, salinity, saturation level of a carbonate phase, or partial pressure of CO_2 (Moore, 1989). These changes are most likely to occur early in the diagenetic history (eogenetic stage), such as the development of a meteoric water system in a shallow shelf sequence; late in the diagenetic history (mesogenetic stage), where hydrocarbon maturation or shale dewatering may provide aggressive fluids; or finally, anytime during burial history, when limestone was exhumed in association with an unconformity (telogenetic stage) and came into contact with meteoric waters (James and Choquette, 1984). However, several authors have mentioned inconsistencies in aragonite dissolution explanations in carbonate rocks worldwide, and that there is a global bias towards meteoric waters as a mechanism for aragonite dissolution (Melim et al., 2002; Melim et al.,

1995; Sanders, 2003; Wright and Cherns, 2004; Wright et al., 2008). Hence, a better understanding of aragonite loss is needed.

The first and most common mechanism used for aragonite dissolution is immersion in meteoric waters. Meteoric waters can occur in a variety of environments, but they are all situated close to surface sediments and settle either as vadose zone or phreatic zone water (James and Choquette, 1984). These waters are corrosive to calcite because of their undersaturation with respect to $CaCO_3$, and increased CO_2 concentrations as a result of their exposure to atmospheric and soil zone CO_2 (Swart, 2015). Because of this, meteoric water dissolution and precipitation produces distinct $\delta^{13}C$ and $\delta^{18}O$ signals. Cements precipitated form meteoric waters contain $\delta^{13}C$ and $\delta^{18}O$ values that are ordinarily depleted, owing that to the origin of the incorporated C and O molecules. These molecules are derived from atmospheric CO_2 and photosynthetic soil CO_2 that are biased towards the lighter carbon isotope (Swart, 2015). Therefore, carbonate cements precipitated from meteoric waters are expected to be depleted in $\delta^{13}C$ and $\delta^{18}O$ relative to their starting marine values. Stable isotope analysis in the Happy Spraberry field revealed relatively enriched values that are similar to typical Permian marine carbonate (figure 4,6). Although cement minerology and texture looked similar to meteoric cements, the stable isotope values clearly suggest precipitation in a marine environment.

Another occurrence of freshwater are offshore vast meteoric ground water reserves (VMGR). It was suggested that vast amounts of meteoric water accumulations in aquifers beneath continental shelves exist and are a common global phenomenon. During sea-level low stands, exposed continental shelves commonly were covered by freshwater lakes and rivers,

which fed ground water aquifers, along with contributions from meteoric water and glacial meltwaters; during sea-level highstands, these VMGRs may underlie marine deposits, and where and when communication is possible, may contribute with freshwaters capable of altering $CaCO_3$ (Post et al., 2013). However, two things must be taken into consideration: 1) their saturation state with regards to $CaCO_3$, and 2) their diagenetic imprint. If these waters traveled long distances before settling, they may be saturated depending upon the route and amount of minerals "picked up". For instance, if these waters were exposed to limestone before reaching aquifers, they may be saturated with respect to $CaCO_3$ and not be reactive enough to cause substantial diagenesis. Nevertheless, if these waters end up altering neighboring marine carbonate sediments, their diagenetic imprint would surely be meteoric-looking. These waters, although they may be more saline than meteoric waters, would have stable isotope signals similar or very close to meteoric waters because they share the same continental and meteoric C and O sources. Because these signals do not occur in the Happy Spraberry dataset, dissolution as a result of offshore freshwater aquifers is considered unlikely.

Another mechanism that can induce aragonite dissolution and that is not restricted to a particular diagenetic stage is microbially induced dissolution. This mechanism is commonly used to explain dissolution in marine waters above the lysocline. Microbial metabolic processes, such as oxidation of organic matter (OM), sulfate reduction, and methanogenesis increase acidity in pore waters, which produces a microenvironment conducive to dissolution of metastable minerals, and consequently creating molds (Frank et al., 2011; Hesse, 1986). Dissolution as a result of microbial metabolic processes, for example, was interpreted in Quaternary periplatform sediments on the slope of the Great Bahama Bank (Malone et al., 2001; Melim et al., 2002), in

surface sediments of the Florida Straits, and in the equatorial Indian Ocean (Schulte and Bard, 2003; Schwarz and Rendle-Bühring, 2005). The oxidation of OM releases CO_2, which reacts with dissolved carbonate ions to form bicarbonate, which is then precipitated as calcite cement (Schwarz and Rendle-Bühring, 2005). However, these microbial processes contribute C with distinct $\delta^{13}C$ values. Oxidation of OM and sulfate reduction may produce carbonate cements with $\delta^{13}C$ values as low as -8‰ VPDB since the source of C is naturally depleted organic matter (-25‰ VPDB; Andrieu et al., 2018; Hesse, 1986; James and Jones, 2015). Methanogenesis is an anaerobic process where carbonate is reduced to produce heavily depleted $\delta^{13}C$ methane (-40 to -60‰ VPDB) and enriched CO_2 (+10‰ VPDB), and depending on ensuing processes, may contribute with heavily depleted or enriched $\delta^{13}C$ values (Dix and Mullins, 1988; Hesse, 1986; Sanders, 2003; Swart, 2015). Also, because this process occurs in anaerobic burial environments, it yields distinct depleted $\delta^{18}O$ values reflecting the higher burial temperatures. Hence the resultant carbonate cement would have to have a $\delta^{13}C$ and $\delta^{18}O$ value that reflects that of the parent OM or its associated processes (Swart, 2015). Because of the absence of heavily depleted $\delta^{13}C$ and $\delta^{18}O$ values, dissolution as a result of microbial metabolic processes in the Happy Spraberry Field is considered unlikely.

A few other models were suggested that explain the selective dissolution of aragonite in marine waters and above its lysocline. For instance, hypersaline waters undersaturated with aragonite was proposed an alternative mechanism to aragonite dissolution in Miocene carbonate rocks in Iraq, Gulf of Suez, and SE Spain (Sun, 1992). However, these waters would induce intense dolomitization and evaporite precipitation, all of which are absent in the Happy Spraberry oolitic succession. Dissolution of aragonite was also interpreted in hard grounds along

the seafloor-sediment interface in Jurassic limestone formations in England and France (Palmer et al., 1988). This model explains dissolution by the natural undersaturation of calcite seas towards aragonite, and where encrusting organisms preserved the shape of the dissolved aragonitic shell in the form of micrite envelopes. The Happy Spraberry oolite succession formed during a Permian ice-house period characterized by aragonitic seas and therefore undersaturation as a result of ocean geochemistry is not a valid mechanism in this study.

We interpret that oomolds were created in a marine environment that may or may not have been located below the aragonite lysocline or ACD. This marine environment, once thought to be insignificant to aragonite dissolution, was usually interpreted as a locus of mainly constructive diagenesis, in the form of cementation and micritization. However, significant dissolution in the Happy Spraberry ooid succession occurred in the marine realm. This environment of dissolution, although mentioned in a few case studies, is not well documented, and has significant implications in the oil industry, and in understanding and reconstructing paleo-oceanic and atmospheric conditions.

5.3. Are oomolds really forming in marine environments?

The Happy Spraberry ooids were deposited within a succession of very well defined slope sediments with characteristic facies as described in section 4.1. Those ooids, which sometimes make up to 75% of rock volume, formed on the platform margin and remobilized to the slope (figure 10) in a manner similar to the shedding process happening today on the western margin of the Great Bahama Bank (Harris et al., 2015; Purkis and Harris, 2016). This is supported by the presence of unorganized grading, clearest in the rudstone/floatstone facies zone;

presence of lithoclasts and mudclasts; the presence of turbidite facies closely underlying and overlying the reservoir. Those ooids were deposited within the deep slope deposits and were not exposed at any point since deposition. This is evident from the clear absence exposure surfaces, in the form of caliche zones, rhizoliths, and karst features, and of the absence of vadose-zone meniscus and/or stalactitic cements. Moreover, the presence of subtidal features such as isopachous cements and micrite envelopes suggests a submersed environment of deposition with no influence of subsequent meteoric diagenesis.

In order for significant dissolution to occur in marine water that is naturally saturated with respect to aragonite, we suggest that dissolution and precipitation occurred at depths within or below the aragonite lysocline (figure 10). Several studies concerned with saturation states of calcite in marine waters observed aragonite dissolution at depths as shallow as 300 m in the Pacific and Atlantic Oceans (Berner et al., 1976; Kerans et al., 1986; Li et al., 1969; Troy et al., 1997). Although typically the ACD occurs at greater depths, it was proposed that at different geologic times the ACD has fluctuated and shoaled significantly (Droxler et al., 1990; Volbers and Henrich, 2002). Since deposition of the Happy Spraberry oolite occurred 4 miles basinward of the Eastern Shelf margin, and with the range of gentle shelf slopes here to be ~1.5-5° (Schlager, 2005), the sediments were likely deposited at a depth of ~170-560 m. It is therefore conceivable that the marine waters responsible for the dissolution of aragonite and precipitation of the LMC equant cements were within the aragonite lysocline or possibly below the ACD.

Another process that may promote a marine environment capable of aragonite dissolution is ocean upwelling. It is the process by which wind-driven forces transport warm ocean surface

waters along coastlines or cause the subduction of surface ocean waters, which are subsequently replaced by colder deep waters (Bao et al., 2017; Lauderdale et al., 2017). Along with wind forces, underwater features such as ridges and mounds can also contribute to the generation of upwelling processes (Bao et al., 2017). This introduction of deep undersaturated waters to shallower environments can cause a major shoaling of the aragonite lysocline, and consequently the dissolution of aragonite at shallow depths. The shoaling of the lysocline along continental margins is well documented, with production rates and microbial processes deemed mainly responsible for the undersaturation (Droxler et al., 1990; Troy et al., 1997; Volbers and Henrich, 2002). However, with the absence of depleted $\delta^{13}C$ and $\delta^{18}O$ values, characteristic of microbially mediated processes, in the Happy Spraberry oolitic facies, ocean upwelling provides a valid explanation for dissolution in marine water.

5.4. Cements and geochemical evidences of marine diagenetic environments

5.4.1. Cement textures

The equant calcite cement (C1), the micrite envelopes (C2), and the isopachous calcite cement (C3) were interpreted to be early diagenetic events. C1 cement is the most abundant cement type. It mainly occludes primary porosity, and sometimes fills secondary porosity. C1 cements mostly are in contact with grains, but occasionally they formed after C3 isopachous cement. Their occurrence as a pore-lining phase around oomoldic, interparticle, and, to a lesser extent, intraparticle pore spaces indicates that their precipitation was an early event, probably occurring soon after deposition and continued during early diagenetic history.

Micrite envelopes are common throughout the studied reservoir and non-reservoir facies. They serve as a major player in porosity preservation and as an indicator of a shallow marine water environment. Micrite envelopes develop as a result of the activities of endolithic organisms that bore the outer shells of allochems, and once they die or vacate their bores, the bores are filled with microcrystalline aragonite or HMC cement (Bathurst, 1966). Although, endolithic borings may occur in a wide range of depths, from the shallow photic zone to the deep abyssal zone, the filling of bores with microcrystalline cement and the development of a micritic envelope is considered a shallow water process because of the lack of micritic precipitates in the deep environments (Golubic et al., 1984; James and Jones, 2015). Micrite envelopes play a significant role in preserving molds because they quickly alter to LMC, and preserve future pore spaces from collapsing.

The Happy Spraberry ooids lack typical meteoric water textures; vadose-zone meniscus and/or stalactitic cements also are absent indicating a submersed environment. Also, exposure surfaces, in the form of caliche zones, and karst features are non-existent. Dolomite C4 and poikilotopic C5 cements were scarce, and interpreted to be late cements because of cross-cutting relationships and because they post-date compaction and breakage.

5.4.2. Precursor aragonite

Bulk rock XRD results, summarized in table 2, show dominant LMC minerology. All samples had bulk rock concentrations of less than 4 w.t.% Mg. The most prominent cement morphology, equant and blocky C1 cement, conforms with typical LMC cements. The three samples that had prominent poikilotopic C5 cements showed distinct celestine content, similar to

findings in the periplatform sediments of the Great Bahama Bank and Maldives (Malone et al., 1990; Melim et al., 2002). It is also worth noting that no aragonite or anhydrite were detected. Although dolomite cement was sporadically present in thin sections, it had no effect on bulk rock mineralogy, as only one sample showed minor traces of dolomite. This is considered an indicator of precursor aragonite, where if the original minerology was HMC, the alteration to LMC should result in the retainment of some Mg in the form of micro-dolomite inclusions (Zempolich and Erba, 1999).

Because of their LMC minerology, C1 and C3 cements are interpreted to be directly linked with the aragonite dissolution event. In order for LMC calcite to be precipitated in a shallow burial environment where pores are most probably saturated with Mg-rich marine waters, LMC saturation as a result of aragonite dissolution must have predominated (Melim et al., 1995; Schlager and James, 1978). This pattern of selective dissolution of aragonite and the precipitation of LMC is common (e.g., Frank et al., 2011; James and Choquette, 1984; Lohmann, 1988; Swart, 2015). In systems that contain aragonite, HMC and LMC, the more soluble phases (aragonite and HMC) are preferentially dissolved, leading to the oversaturation and precipitation of the least-soluble phase (LMC), which leads to further undersaturation with respect to aragonite and HMC (figure 11). This system could theoretically dissolve all metastable phases and precipitate the more stable LMC until all metastable minerals are consumed (Swart, 2015).

The relationship between cement morphology and mineralogy indicates that the main control over cement morphology is the Mg/Ca ratio of the precipitating water, where low Mg/Ca ratios prefer the precipitation of equant crystals, and high Mg/Ca ratios prefer the precipitation of

elongate, acicular to bladed crystals (Given and Wilkinson, 1985; Swart, 2015). However, the interpreted marine LMC cements in the Happy Spraberry field are mostly of an equant texture. This again suggests that aragonite, which is heavily depleted in Mg, is the main source of LMC. In order to attain the required LMC saturation, this process also requires the environment of dissolution and precipitation to be relatively restricted from active sea-water circulation to prevent the mass exportation of dissolved aragonite. This will ensure the buildup of sufficient LMC to achieve supersaturation and precipitation.

Trace element analysis of cements also provides evidence of precursor aragonite. Typical Sr values for LMC cements precipitated from active seawater of 25^{o}C average 500 ppm (Melim et al., 2002). Sr concentrations in the Happy Spraberry equant cements are relatively elevated, with a mean concentration of 605 ppm. The relatively elevated Sr content is considered common of marine environments (Zempolich and Erba, 1999). Furthermore, the elevated Sr concentrations (>500 ppm) can be attributed to the dissolution of aragonitic allochems, locally ooids, and the incorporation of Sr into LMC cement. This signal commonly is considered a good indicator of precursor aragonite (Sandberg, 1985; Zempolich and Erba, 1999). The elevated Sr concentrations in the Happy Spraberry field components suggest precipitation within a semi-restricted environment capable of retaining Sr from active marine water circulation. Samples that show even higher Sr concentrations (>1000 ppm) and/or sporadic precipitation of celestine are muddier facies of packstone/wackstone with more conspicuous micritization of ooids. These samples suggest a relatively more restricted micro-environment capable of preserving Sr from being subsequently flushed.

5.4.3. Marine cement signals

Four types of samples were analyzed for trace elements concentrations: equant blocky C1 cements, isopachous C3 cements, micritized ooids, and brachiopod shells. They showed distinctly low Mn content and relatively elevated Sr content. Mn concentrations averaged 57 ppm, with a maximum value of 170 ppm. Sr concentrations averaged 605 ppm, with a maximum value of *ca* 2330 ppm. This response is typical of marine carbonate cements (Zempolich and Erba, 1999).

Another important indicator of marine water geochemistry is Fe concentrations. Fe was relatively low in all samples, with the vast majority of samples in the range of 200-400 ppm. The low Fe and aforementioned Mn concentrations also point away from an exposure or vadose setting. Because they would be situated close to soil horizons, cements in exhumed surfaces or vadose zones are expected to have elevated concentrations of Fe and Mn of about 1000 ppm (Swart, 2015). Even with the absence of dense soil horizons, these elements can accumulate from aeolian deposits originating from close to remote terrestrial locations (Rossinsky Jr et al., 1992). These well-defined low concentrations of Fe and Mn further argue against an interpretation of a meteoric water environment.

Mg values had a wider range, but all cements and grains had <4 % Mg concentrations. The precipitation of LMC in marine and shallow burial settings is not unlikely and were described thoroughly in literature (e.g., Heydari et al., 1993; Melim et al., 1995; Schlager and James, 1978).

Sodium concentrations show clear dependence on cement/grain types. The lowest Na concentrations are characteristic of the equant blocky cements, and the isopachous cements. They show a range of 105-604 ppm, with an average of 315 ppm. Brachiopod shells showed higher Na concentrations, with an average of 1184 ppm. Meanwhile the highest concentrations are those of micrite, which have average Na concentrations of 1377 ppm. Sodium was the only element that was able to segregate the cement/grain types into distinctive zones. An explanation for this is possibly that biogenic calcite commonly is more enriched in Na, whereas diagenetic LMC, as a result of dissolution and re-precipitation, tends to show lower concentrations of Na (Malone et al., 1990).

29 samples from the oolite-rich succession from 8 wells were chosen for stable isotope analysis. In order to accurately evaluate the isotopic ratios of diagenesis, an essential first step is the estimation of the starting composition of the marine carbonate. Such estimates are essential to provide a baseline relative to which the effects of diagenesis can be evaluated (Meyers and Lohmann, 1985). Many studies have documented variations in isotopic compositions of marine carbonate through geologic time (e.g., Grossman et al., 2008; Korte et al., 2008; Lohmann and Walker, 1989), and because of their resistance to alteration, stable isotopic ratios of diagenetically unaltered brachiopod shells often are used as reflections of contemporaneous seawater geochemistry (Grossman et al., 2008; Korte et al., 2008). For the purpose of this study, a mean range was derived with more weight given to Grossman et al. (2008) averages because the samples used are from the Permian Basin in Texas, which is more analogous with the current study succession. The mean ratios for $\delta^{13}C$ and $\delta^{18}O$ for unaltered Early Permian brachiopods

was 4.6‰ VDPB and -3.1‰ VPDB respectively (Grossman et al., 2008). Isotopic ratios of brachiopod shells sampled from this reservoir (figure 6) fall within the established Permian marine carbonate ranges. They showed $\delta^{13}C$ values of ~3.9‰ VDPB and a $\delta^{18}O$ range of -3.5‰ to -2.9‰ VDPB. This increases confidence in the isotope ratios sampled, and establishes that the ambient waters at the Happy Spraberry Field are geochemically similar to coeval paleo-oceans and seas. These obtained values were also used to define a more accurate marine carbonate isotope range representative of this field. The mean range of $\delta^{13}C$ for Permian marine carbonates was chosen at 3.5‰ to 4.5‰ VPDB, and the mean range for $\delta^{18}O$ for Permian marine carbonates was chosen at -3.5‰ to -2.5‰ VPDB.

After establishing a baseline of Permian marine carbonate stable isotope values, the main purpose was to analyze the "meteoric-looking" equant cement. These early LMC cements show values that confirm the marine origin of those crystals, which also reflects the isotopic ratios of the diagenetic environment where oomoldic porosity was created.

The isotope ratios show little spread, and although most fall within the defined 'acceptable' marine carbonate range (18 of 29), some samples showed slightly heavier $\delta^{18}O$ signals (figure 6). There are a few possible reasons for these heavier $\delta^{18}O$ values. Since aragonite tends to have a slightly heavier $\delta^{18}O$ signal than calcite, this would point to the original composition of the leached ooids was indeed aragonite (and not HMC). Dolomite, where present, may also contribute to an increased $\delta^{18}O$ signal because dolomite is naturally more enriched in $\delta^{18}O$ relative to LMC formed under the same conditions (Swart, 2015). However, dolomite was very either scarce or absent in all samples, and thus could not have contributed to a

heavier $\delta^{18}O$ signal. Finally, the heavier $\delta^{18}O$ signal could also point to cold or evaporative waters. Since, there is no evidence to support precipitation from highly evaporative waters (e.g. intense dolomitization, anhydrite cements/nodules), it is more plausible that the waters were of a colder marine origin. Therefore, we propose that the reason behind those relatively enriched $\delta^{18}O$ signals is precursor aragonite and possibly cooler marine water.

Colder marine waters would have to be deeper and probably undersaturated with respect to aragonite. Using the revised Epstein et al. (1953) paleo-temperature equation we calculate crystallization at temperatures ranging from 27-17 degrees. Based on ocean thermocline measurements, this possibly could place deposition at a depth of more than 500 m. It is therefore conceivable that the marine waters responsible for the dissolution of aragonite and precipitation of the LMC equant cements were within the aragonite lysocline or possibly below the ACD. Although typically the ACD occurs at greater depths, it was proposed that at different geologic times the ACD has fluctuated and shallowed significantly (Droxler et al., 1990; Volbers and Henrich, 2002).

5.5. Implications

The dissolution of aragonite in marine waters within or above the aragonite lysocline has major implications in interpreting the carbonate rock record. One possible consequence is the taphonomic bias against aragonitic organisms, where a higher proportion of calcitic or bimineralic organisms are preserved and represented in the sedimentary record. This may lead to misunderstandings of paleo-ecosystems and depositional conditions. For instance, significant loss of diversity in Lower Jurassic aragonitic faunas was observed in South Wales between

silicified and non-silicified fauna (Wright et al., 2003), suggesting that early silicification prevented aragonite dissolution and preserved original diversity. Another consequence is the artificial skewing of sedimentation and accumulation rates by aragonite loss in conditions once thought insignificant or unconducive to aragonite dissolution. This can be seen, for instance, by the low sedimentation rates calculated for cool-water systems, in which aragonite dissolution may have played a major role (James et al., 2005). Dissolution is also accounted for in calculations of ocean $CaCO_3$ production rates, and therefore the carbon budget calculation. Because these values are derived from accumulation rates, a correction factor was suggested to account for the dissolution of aragonite above the lysocline (Martin and Sayles, 1996). Lastly, carbonate dissolution is often factored in when reconstructing ocean pH variations through geologic time, which has major implications in understanding past changes of atmospheric pCO_2 (Schulte and Bard, 2003).

It is also a common practice in the oil industry to interpret and reconstruct the depositional system of reservoirs and their ensuing diagenetic events in order to better understand and predict the petrophysical properties of the reservoir. This reconstruction leads to the modeling and extrapolation of properties, which leads to the development of exploitation schemes. Acknowledging the possibility of aragonite dissolution in marine waters would prevent erroneous interpretations of moldic porosity to be of definite meteoric-associated environments. A more accurate interpretation of depositional and diagenetic environments would lead interpreters to a more accurate prediction of porosity and permeability distribution and geometry. Those results have a significant economic impact since oolites comprise a large proportion of the world's carbonate hydrocarbon reservoirs (Flügel, 2013; Lehrmann et al.,

2012). Consequently, associated oomoldic porosity is a major contributor to hydrocarbon production from major plays across the globe. Oomoldic pore systems (usually high porosity and low permeability) occur in the Jurassic Smackover reservoirs, which commonly are also dolomitic (Moore and Druckman, 1981), the Ste. Genevieve Limestone in Kentucky in which oolitic bimodal (primary and secondary) porosity reservoirs are prominent (Asquith, 1986), and the Fullerton Field in west Texas which owes much of its production to Lower Permian oomoldic grainstone and packstone facies (Ruppel and Jones, 2006). Other significant occurrences of hydrocarbon-rich reservoirs characterized with prominent oomoldic porosity in the United States include the Mississippian units in the Anadarko Basin and Hugoton Embayment, the Greenbrier and Monteagle limestones of the Appalachian Basin, and the Madison Group of the Williston Basin (Keith and Zuppann, 1993). The Jurassic Arab-D reservoir of the Ghawar field in Saudi Arabia is one of the largest oil bearing oolitic formations in the world. It has a bimodal porosity scheme, with oomoldic pores contributing to better reservoir zones (Lindsay et al., 2006).

6. CONCLUSION

The present study of oomoldic porosity in the Happy Spraberry Field of West Texas provides evidence for dissolution of aragonitic ooids and the precipitation of equant LMC cements in a marine environment. This was observed in the oolitic grainstone and packstone facies, and early cements were identified as key to interpret the diagenetic environment that induced the dissolution of ooids and precipitation of LMC cement. Three early cement types were identified: 1) equant blocky low-Mg calcite, 2) micrite envelopes, and 3) isopachous low-Mg calcite. These cements showed textures of both meteoric and shallow marine settings. Isopachous cements and micrite envelopes suggest a marine environment, while the equant blocky cement appears like typical meteoric cement. However, these geometries are not considered diagnostic as pointed out by many.

Most stable isotope values are within the acceptable range of Permian marine carbonates ($\delta^{13}C$ = 3.5 to 4.5‰, $\delta^{18}O$ = -3.5 to -2.5‰), whereas the remaining samples (11 of 29) showed slightly heavier $\delta^{18}O$ values (up to -1.5‰). This may be due to the contribution of precursor aragonite, which contributes with relatively enriched $\delta^{18}O$ values, and/or that dissolution and precipitation occurred in colder marine waters. Crystallization paleo-temperatures were calculated at 17-27°C.

Trace elements analysis of the equant blocky cements, isopachous cements, micritized ooids, and brachiopods points to a marine geochemistry. Most notable are the elevated Sr concentrations and the distinctly low Mn concentrations. Sr and Mn averaged 605 ppm and 56 ppm respectively for all samples, which is typical of marine carbonate. Furthermore, some

samples showed even higher Sr concentrations (up to 2332 ppm), which if paired with the abundant oomolds, is considered a good indicator of precursor aragonite.

Whether or not this dissolution happens below or above the aragonite lysocline is a matter of further debate, but what is evident is that aragonite is prone to dissolution early after its formation. Marine-water dissolution of aragonite often is explained by seawater geochemistry, alluding to calcite seas being undersaturated with respect to aragonite and promoting its dissolution. However, aragonite dissolution in marine waters was also evident in aragonite seas, as seen in this study, as well as in present-day seawater. This suggests that while the chemistry of oceans and seas as a whole plays a role in promoting or inhibiting dissolution, it is not the only factor. The dissolution of aragonite in marine waters is probably more common in the rock record than once suspected and therefore more open-mindedness is required when interpreting diagenetic processes relating to oomoldic or moldic porosity.

Although meteoric diagenesis may be the most common cause of oomolds, it certainly is not the only one. Alternative mechanisms may induce aragonite dissolution and the creation of oomoldic porosity, and the data from the Happy Spraberry Field suggest that the mechanisms behind the dissolution of ooids and the precipitation of LMC equant cements occurred in a subtidal marine setting. Marine signatures are evident in mineralogy, C and O stable isotope values, and elemental composition. Without independent evidence such as caliche horizons, vadose fabrics, or stable isotope and geochemical data, equant sparry calcite cement cannot unequivocally be attributed to meteoric origins.

REFERENCES

AHR, W. M. & HAMMEL, B. S. 1999. Identification and Mapping of Flow Units in Carbonate Reservoirs an Example from the Happy Spraberry (Permian) Field Garza County, Texas USA. *Energy exploration & exploitation,* 17**,** 311-334.

ANDRIEU, S., BRIGAUD, B., BARBARAND, J. & LASSEUR, E. 2018. The complex diagenetic history of discontinuities in shallow-marine carbonate rocks: New insights from high-resolution ion microprobe investigation of δ18O and δ13C of early cements. *Sedimentology,* 65**,** 360-399.

ASQUITH, G. B. 1986. Microporosity in the O'Hara Oolite zone of the Mississippian Ste. Genevieve Limestone, Hopkins County, Kentucky, and its implications for formation evaluation. *Carbonates and Evaporites,* 1**,** 7.

ATCHLEY, S. C., KOZAR, M. G. & YOSE, L. A. 1999. A predictive model for reservoir distribution in the Permian (Leonardian) Clear Fork and Glorieta formations, Robertson field area, west Texas. *AAPG bulletin,* 83**,** 1031-1056.

BAO, S., LI, X., SHEN, D., YANG, Z., PIETRAFESA, L. J. & ZHENG, W. 2017. Ocean upwelling along the Yellow Sea coast of China revealed by satellite observations and numerical simulation. *IEEE Transactions on Geoscience and Remote Sensing,* 55**,** 526-536.

BATHURST, R. 1966. Boring algae, micrite envelopes and lithification of molluscan biosparites. *Geological Journal,* 5**,** 15-32.

BERNER, R. A., BERNER, E. K. & KEIR, R. S. 1976. Aragonite dissolution on the Bermuda Pedestal: its depth and geochemical significance. *Earth and Planetary Science Letters,* 30**,** 169-178.

BOSELLINI, A., MASETTI, D. & SARTI, M. 1981. A Jurassic "Tongue of the ocean" infilled with oolitic sands: the Belluno Trough, Venetian Alps, Italy. *Marine Geology,* 44**,** 59-95.

BROWN, T. C. 1914. Origin of oolites and the oolitic texture in rocks. *Bulletin of the Geological Society of America,* 25**,** 745-780.

BURNE, R. V., EADE, J. C. & PAUL, J. 2012. The Natural History of Ooliths: Franz Ernst Brückmann's treatise of 1721 and its significance for the understanding of oolites. *Hallesches Jb. Geowiss,* 35**,** 93-114.

CHOQUETTE, P. W. & PRAY, L. C. 1970. Geologic nomenclature and classification of porosity in sedimentary carbonates. *AAPG bulletin,* 54**,** 207-250.

CLAYTON, J. L. 2011. *Stratigraphy and reservoir architecture of a Permian toe-of-slope ooid fan, Happy (Spraberry) Field, Garza Co., Texas.*

CLOUD, P., BARNES, V. E., BRIDGE, J. & WARREN, L. 1945. *Stratigraphy of the Ellenburger Group in Central Texas: A Progress Report*, The University.

COLE, T. 1942. Subsurface study of Ellenburger Formation in West Texas. *AAPG Bulletin,* 26**,** 1398-1409.

CROWLEY, A. J. & HENDRICKS, L. 1945. Lower Ordovician and Upper Cambrian subsurface subdivisions in north-central Texas. *AAPG Bulletin,* 29**,** 413-425.

DAHANAYAKE, K., GERDES, G. & KRUMBEIN, W. E. 1985. Stromatolites, oncolites and oolites biogenically formed in situ. *Naturwissenschaften,* 72**,** 513-518.

DEFORD, R. K. & WALDSCHMIDT, W. A. 1946. Oolite and oolith. *AAPG Bulletin,* 30**,** 1587-1588.

DIX, G. R. & MULLINS, H. T. 1988. Rapid burial diagenesis of deep-water carbonates: Exuma Sound, Bahamas. *Geology,* 16**,** 680-683.

DROXLER, A., HADDAD, G., MUCCIARONE, D. & CULLEN, J. 1990. Pliocene-Pleistocene aragonite cyclic variations in Ocean Drilling Program holes 714A and 716B (the Maldives) compared to hole 633A (the Bahamas): records of climate-induced CaCO 3 preservation at intermediatewater depths. *Procedings of the Ocean Drilling Program, Scientific Results: Ocean Drilling Program, Texas A&M University, College Station, Texas*.

EPSTEIN, S., BUCHSBAUM, R., LOWENSTAM, H. A. & UREY, H. C. 1953. Revised carbonate-water isotopic temperature scale. *Geological Society of America Bulletin,* 64**,** 1315-1326.

FLÜGEL, E. 2013. *Microfacies of carbonate rocks: analysis, interpretation and application*, Springer Science & Business Media.

FRANK, T. D., TITSCHACK, J. & THIERENS, M. 2011. Aragonite loss in a cold-water coral mound: mechanisms and implications. *Sedimentology,* 58**,** 670-690.

GENTRY, M. D. 2005. *Applications of artificial neural networks in the identification of flow units, Happy Spraberry Field, Garza County, Texas.* Texas A&M University.

GIVEN, R. K. & WILKINSON, B. H. 1985. Kinetic control of morphology, composition, and mineralogy of abiotic sedimentary carbonates. *Journal of Sedimentary Research,* 55**,** 109-119.

GOLUBIC, S., CAMPBELL, S., DROBNE, K., CAMERON, B., BALSAM, W. L., CIMERMAN, F. & DUBOIS, L. 1984. Microbial endoliths: a benthic overprint in the sedimentary record, and a paleobathymetric cross-reference with foraminifera. *Journal of Paleontology***,** 351-361.

GROSSMAN, E. L., YANCEY, T. E., JONES, T. E., BRUCKSCHEN, P., CHUVASHOV, B., MAZZULLO, S. & MII, H.-S. 2008. Glaciation, aridification, and carbon sequestration in the Permo-Carboniferous: the isotopic record from low latitudes. *Palaeogeography, Palaeoclimatology, Palaeoecology,* 268**,** 222-233.

HAMMEL, B. 1996. High resolution reservoir characterization of the Permian (upper Leonardian) Spraberry Formation. *Happy Spraberry Field, Garza County, Texas: Unpublished Master's Thesis, Texas A&M University*.

HANDFORD, C. R. 1981. Sedimentology and genetic stratigraphy of Dean and Spraberry formations (Permian), Midland basin, Texas. *AAPG Bulletin,* 65**,** 1602-1616.

HARRIS, P., DIAZ, M. R. & EBERLI, G. P. 2018. The Formation and Distribution of Modern Ooids on Great Bahama Bank. *Annual review of marine science*.

HARRIS, P. M., PURKIS, S. J., ELLIS, J., SWART, P. K. & REIJMER, J. J. 2015. Mapping bathymetry and depositional facies on Great Bahama Bank. *Sedimentology,* 62**,** 566-589.

HESSE, R. 1986. Diagenesis# 11. Early diagenetic pore water/sediment interaction: modern offshore basins. *Geoscience Canada,* 13.

HEYDARI, E., SNELLING, R. D., DAWSON, W. C. & MACHAIN, M. L. 1993. Ooid Mineralogy and Diagenesis of the Pitkin Formation, North-Central Arkansas: Chapter 13.

JAMES, N. P., BONE, Y. & KYSER, T. K. 2005. Where has all the aragonite gone? Mineralogy of Holocene neritic cool-water carbonates, southern Australia. *Journal of Sedimentary Research,* 75**,** 454-463.

JAMES, N. P. & CHOQUETTE, P. W. 1984. Diagenesis 9. Limestones-the meteoric diagenetic environment. *Geoscience Canada.*

JAMES, N. P. & JONES, B. 2015. *Origin of Carbonate Rocks*, John Wiley & Sons.

KALKOWSKY, E. 1908. Oolith und Stromatolith im norddeutschen Buntsandstein. *Zeitschrift der deutschen geologischen Gesellschaft***,** 68-125.

KEITH, B. D. & ZUPPANN, C. W. 1993. Mississippian oolites and petroleum reservoirs in the United States—An overview. *Mississippian oolites and modern analogs: AAPG Studies in Geology,* 35**,** 1-12.

KERANS, C., HURLEY, N. F. & PLAYFORD, P. E. 1986. Marine diagenesis in Devonian reef complexes of the Canning Basin, Western Australia. *Reef diagenesis.* Springer.

KORTE, C., JONES, P. J., BRAND, U., MERTMANN, D. & VEIZER, J. 2008. Oxygen isotope values from high-latitudes: Clues for Permian sea-surface temperature gradients and Late Palaeozoic deglaciation. *Palaeogeography, Palaeoclimatology, Palaeoecology,* 269**,** 1-16.

LAUDERDALE, J. M., WILLIAMS, R. G., MUNDAY, D. R. & MARSHALL, D. P. 2017. The impact of Southern Ocean residual upwelling on atmospheric CO 2 on centennial and millennial timescales. *Climate Dynamics,* 48**,** 1611-1631.

LAYMAN, J. M. 2004. *Porosity Characterization Utilizing Petrographic Image Analysis: Implications for Identifying and Ranking Reservoir Flow Units, Happy Spraberry Field, Garza County, Texas.* Texas A&M University.

LEHRMANN, D. J., MINZONI, M., LI, X., YU, M., PAYNE, J. L., KELLEY, B. M., SCHAAL, E. K. & ENOS, P. 2012. Lower Triassic oolites of the Nanpanjiang Basin, south China: Facies architecture, giant ooids, and diagenesis—Implications for hydrocarbon reservoirs. *AAPG bulletin,* 96**,** 1389-1414.

LI, Y. H., TAKAHASHI, T. & BROECKER, W. S. 1969. Degree of saturation of CaCO3 in the oceans. *Journal of Geophysical Research,* 74**,** 5507-5525.

LINDSAY, R. F., CANTRELL, D. L., HUGHES, G. W., KEITH, T. H., MUELLER III, H. W. & RUSSELL, S. D. 2006. Ghawar Arab-D reservoir: widespread porosity in shoaling-upward carbonate cycles, Saudi Arabia.

LOHMANN, K. C. 1988. Geochemical patterns of meteoric diagenetic systems and their application to studies of paleokarst. *Paleokarst.* Springer.

LOHMANN, K. C. & WALKER, J. C. 1989. The δ18O record of Phanerozoic abiotic marine calcite cements. *Geophysical Research Letters,* 16**,** 319-322.

LONGMAN, M. W. 1980. Carbonate diagenetic textures from nearsurface diagenetic environments. *AAPG bulletin,* 64**,** 461-487.

LYELL, C. 1855. *A manual of elementary geology*, Murray.

MALONE, M. J., BAKER, P. A., BURNS, S. J. & SWART, P. K. Geochemistry of periplatform carbonate sediments, Leg 115, Site 716 (Maldives Archipelago, Indian Ocean). Proceedings of the Ocean Drilling Program, Scientific Results, 1990. Ocean Drilling Program, 647-659.

MALONE, M. J., SLOWEY, N. C. & HENDERSON, G. M. 2001. Early diagenesis of shallow-water periplatform carbonate sediments, leeward margin, Great Bahama Bank (Ocean Drilling Program Leg 166). *GSA Bulletin,* 113**,** 881-894.

MARIOTTI, G., O'REILLY, S., WINTER, A., NEWMAN, S., PRUSS, S., BOSAK, T., KLEPAC-CERAJ, V., MCDERMOTT, F. & SUMMONS, R. Molecular evidence for a microbial role in ooid formation and preservation of molecular biosignatures in ancient oolite. AGU Fall Meeting Abstracts, 2015.

MARTIN, W. & SAYLES, F. 1996. CaCO3 dissolution in sediments of the Ceara Rise, western equatorial Atlantic. *Geochimica et Cosmochimica Acta,* 60**,** 243-263.

MAZINGUE-DESAILLY, V. P. G. 2004. *Assessing the influence of diagenesis on reservoir quality: Happy Spraberry Field, Garza County, Texas.* Texas A&M University.

MAZZULLO, S. 1995. Permian Stratigraphy and Facies, Permian Basin (Texas—New Mexico) and Adjoining Areas in the Midcontinent United States. *The Permian of Northern Pangea.* Springer.

MCQUEEN, H. S. 1931. *Insoluble residues as a guide in stratigraphic studies*, Missouri Bureau of Geology and Mines.

MELIM, L., WESTPHAL, H., SWART, P., EBERLI, G. & MUNNECKE, A. 2002. Questioning carbonate diagenetic paradigms: evidence from the Neogene of the Bahamas. *Marine Geology,* 185**,** 27-53.

MELIM, L. A., SWART, P. K. & MALIVA, R. G. 1995. Meteoric-like fabrics forming in marine waters: Implications for the use of petrography to identify diagenetic environments. *Geology,* 23**,** 755-758.

MEYERS, W. J. & LOHMANN, K. C. 1985. Isotope geochemistry of regionally extensive calcite cement zones and marine components in Mississippian limestones, New Mexico.

MILLIMAN, J., TROY, P., BALCH, W., ADAMS, A., LI, Y.-H. & MACKENZIE, F. 1999. Biologically mediated dissolution of calcium carbonate above the chemical lysocline? *Deep Sea Research Part I: Oceanographic Research Papers,* 46**,** 1653-1669.

MOORE, C. H. 1989. *Carbonate diagenesis and porosity*, Elsevier.

MOORE, C. H. & DRUCKMAN, Y. 1981. Burial diagenesis and porosity evolution, upper Jurassic Smackover, Arkansas and Louisiana. *Aapg Bulletin,* 65**,** 597-628.

PALMER, T. & WILSON, M. 2004. Calcite precipitation and dissolution of biogenic aragonite in shallow Ordovician calcite seas. *Lethaia,* 37**,** 417-427.

PALMER, T. J., HUDSON, J. & WILSON, M. A. 1988. Palaeoecological evidence for early aragonite dissolution in ancient calcite seas. *Nature,* 335**,** 809-810.

POST, V. E., GROEN, J., KOOI, H., PERSON, M., GE, S. & EDMUNDS, W. M. 2013. Offshore fresh groundwater reserves as a global phenomenon. *Nature,* 504**,** 71.

PURKIS, S. J. & HARRIS, P. M. 2016. The extent and patterns of sediment filling of accommodation space on Great Bahama Bank. *Journal of Sedimentary Research,* 86**,** 294-310.

REID, R. P. & MACINTYRE, I. G. 1998. Carbonate recrystallization in shallow marine environments: a widespread diagenetic process forming micritized grains. *Journal of Sedimentary Research,* 68**,** 928-946.

RICHTER, D. K. 1983. Calcareous ooids: a synopsis. *Coated grains.* Springer.

ROSSINSKY JR, V., WANLESS, H. R. & SWART, P. K. 1992. Penetrative calcretes and their stratigraphic implications. *Geology,* 20**,** 331-334.

RUPPEL, S. C. & JONES, R. H. 2006. Key role of outcrops and cores in carbonate reservoir characterization and modeling, Lower Permian Fullerton field, Permian Basin, United States.

SALLER, A. H. 1986. Radiaxial calcite in lower Miocene strata, subsurface Enewetak Atoll. *Journal of Sedimentary Research,* 56**,** 743-762.

SANDBERG, P. 1985. Aragonite cements and their occurrence in ancient limestones.

SANDERS, D. 2003. Syndepositional dissolution of calcium carbonate in neritic carbonate environments: geological recognition, processes, potential significance. *Journal of African Earth Sciences,* 36**,** 99-134.

SARG, J., MARKELLO, J. & WEBER, L. 1999. The second-order cycle, carbonate-platform growth, and reservoir, source, and trap prediction.

SCHLAGER, W. 2005. *Carbonate sedimentology and sequence stratigraphy*, SEPM Soc for Sed Geology.

SCHLAGER, W. & JAMES, N. 1978. Low-magnesian calcite limestones forming at the deep-sea floor, Tongue of the Ocean, Bahamas. *Sedimentology,* 25**,** 675-702.

SCHOLLE, P. A. & ULMER-SCHOLLE, D. S. 2003. *A Color Guide to the Petrography of Carbonate Rocks: Grains, Textures, Porosity, Diagenesis, AAPG Memoir 77*, AAPG.

SCHULTE, S. & BARD, E. 2003. Past changes in biologically mediated dissolution of calcite above the chemical lysocline recorded in Indian Ocean sediments. *Quaternary science reviews,* 22**,** 1757-1770.

SCHWARZ, J. & RENDLE-BÜHRING, R. 2005. Controls on modern carbonate preservation in the southern Florida Straits. *Sedimentary Geology,* 175**,** 153-167.

SIMONE, L. 1980. Ooids: a review. *Earth-Science Reviews,* 16**,** 319-355.

SORBY, H. C. 1879. The structure and origin of limestones. *The Popular science review,* 3**,** 134-137.

STANLEY, S. M. & HARDIE, L. A. 1998. Secular oscillations in the carbonate mineralogy of reef-building and sediment-producing organisms driven by tectonically forced shifts in seawater chemistry. *Palaeogeography, Palaeoclimatology, Palaeoecology,* 144**,** 3-19.

SUN, S. Q. 1992. Skeletal aragonite dissolution from hypersaline seawater: a hypothesis. *Sedimentary Geology,* 77**,** 249-257.

SWART, P. K. 2015. The geochemistry of carbonate diagenesis: The past, present and future. *Sedimentology,* 62**,** 1233-1304.

TAN, X., ZHAO, L., LUO, B., JIANG, X., CAO, J., LIU, H., LI, L., WU, X. & NIE, Y. 2012. Comparison of basic features and origins of oolitic shoal reservoirs between carbonate platform interior and platform margin locations in the Lower Triassic Feixianguan Formation of the Sichuan Basin, Southwest China. *Petroleum Science,* 9**,** 417-428.

TEICHERT, C. 1970. Oolite, oolith, ooid: discussion. *AAPG Bulletin,* 54**,** 1748-1749.

TROY, P. J., LI, Y.-H. & MACKENZIE, F. T. 1997. Changes in surface morphology of calcite exposed to the oceanic water column. *Aquatic Geochemistry,* 3**,** 1-20.

TUCKER, M. E. & WRIGHT, V. P. 1990. Carbonate sedimentology.

VEIZER, J. & MACKENZIE, F. 2003. Evolution of sedimentary rocks. *Treatise on geochemistry,* 7**,** 407.

VOLBERS, A. N. & HENRICH, R. 2002. Late Quaternary variations in calcium carbonate preservation of deep-sea sediments in the northern Cape Basin: results from a multiproxy approach. *Marine Geology,* 180**,** 203-220.

WARD, R. F., KENDALL, C. G. S. C. & HARRIS, P. M. 1986. Upper Permian (Guadalupian) facies and their association with hydrocarbons--Permian basin, west Texas and New Mexico. *AAPG Bulletin,* 70**,** 239-262.

WRIGHT, P. & CHERNS, L. 2004. Are there" black holes" in carbonate deposystems? *Geologica Acta,* 2**,** 285.

WRIGHT, P., CHERNS, L. & HODGES, P. 2003. Missing molluscs: field testing taphonomic loss in the Mesozoic through early large-scale aragonite dissolution. *Geology,* 31**,** 211-214.

WRIGHT, V. P., CHERNS, L., LUKASIK, J. & SIMÓ, A. 2008. The subtle thief: selective dissolution of aragonite during shallow burial and the implications for carbonate sedimentology. *Controls on Carbonate Platform and Reef Development: SEPM, Special Publication,* 89**,** 47-54.

YANG, K.-M. & DOROBEK, S. L. 1995. The Permian basin of west Texas and New Mexico: tectonic history of a" composite" foreland basin and its effects on stratigraphic development. *Stratigraphic evolution of foreland basins: SEPM Special Publication,* 52**,** 149-174.

ZEMPOLICH, W. G. & ERBA, E. 1999. Sedimentologic and chemostratigraphic recognition of third-order sequences in resedimented carbonate: the Middle Jurassic Vajont Limestone, Venetian Alps, Italy.

APPENDIX A

FIGURES

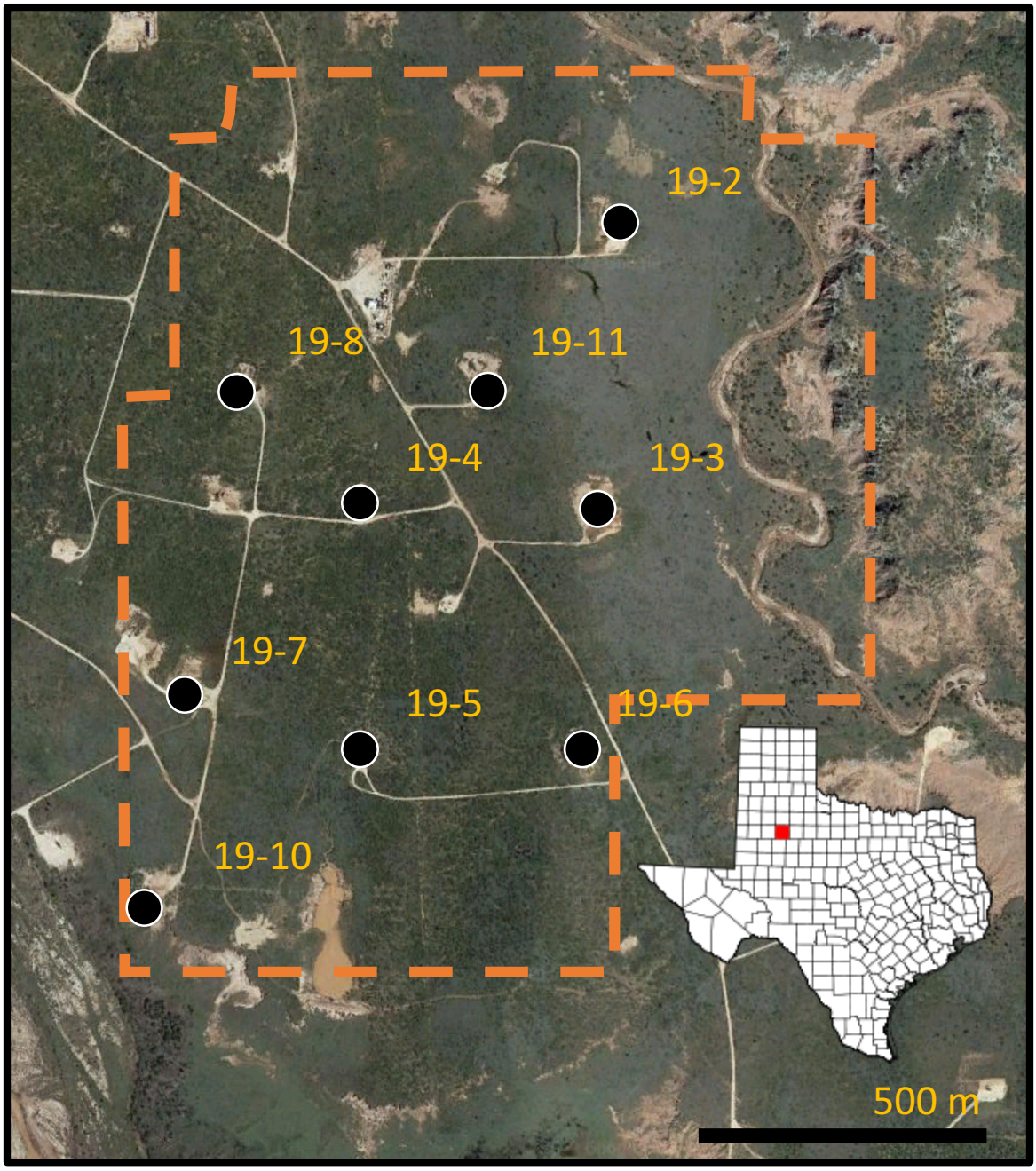

Figure 1. Location map of the Happy Spraberry Field, in Garza County, Texas. More than 20 wells were drilled. Only wells utilized in this study are displayed.

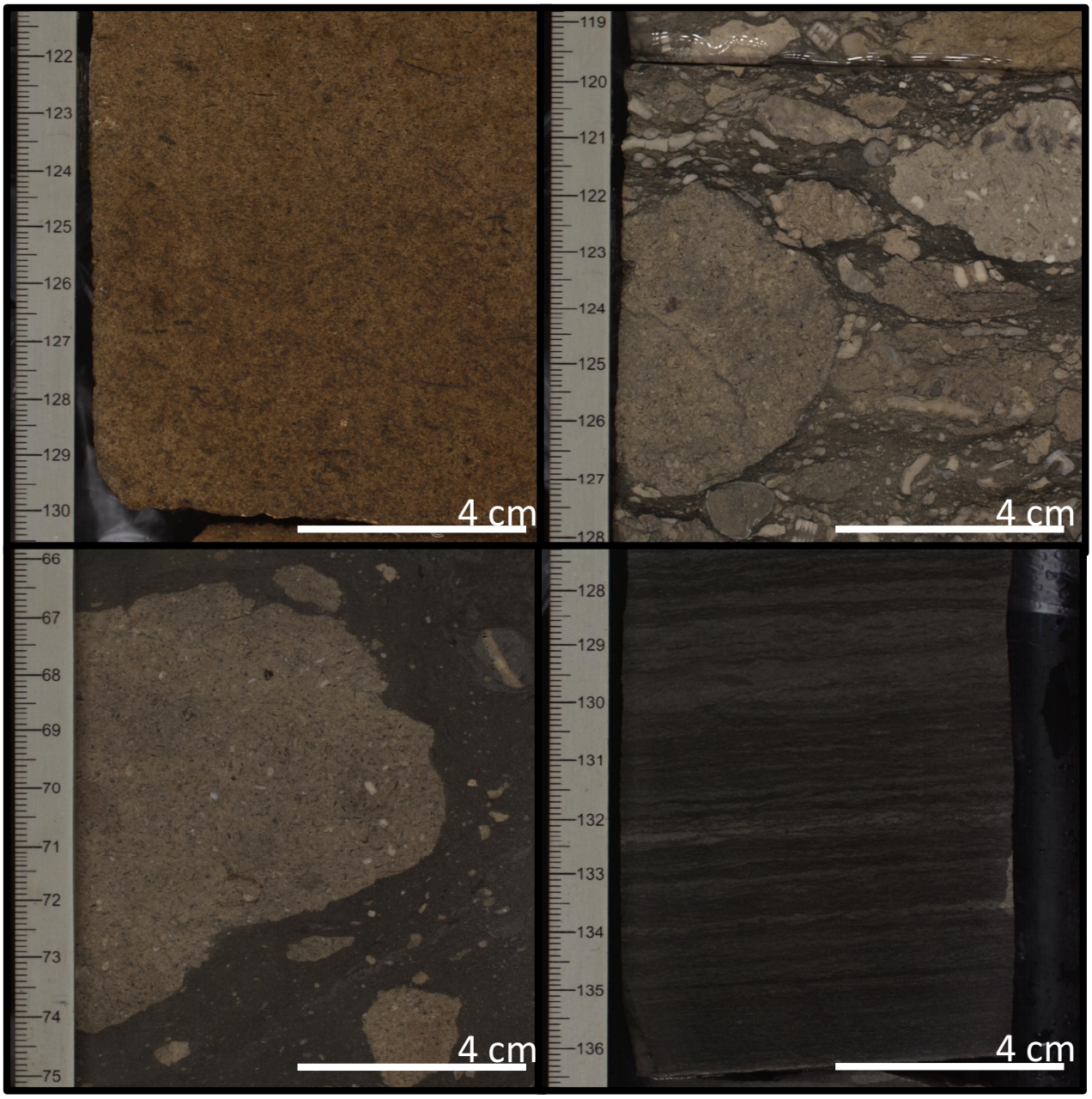

Figure 2. Core photos of 4 interpreted facies in the Happy Spraberry succession. A) Typical oolitic grainstone facies. B) Skeletal rudstone facies. C) Skeletal floatstone facies. D) Shaly siltstone facies.

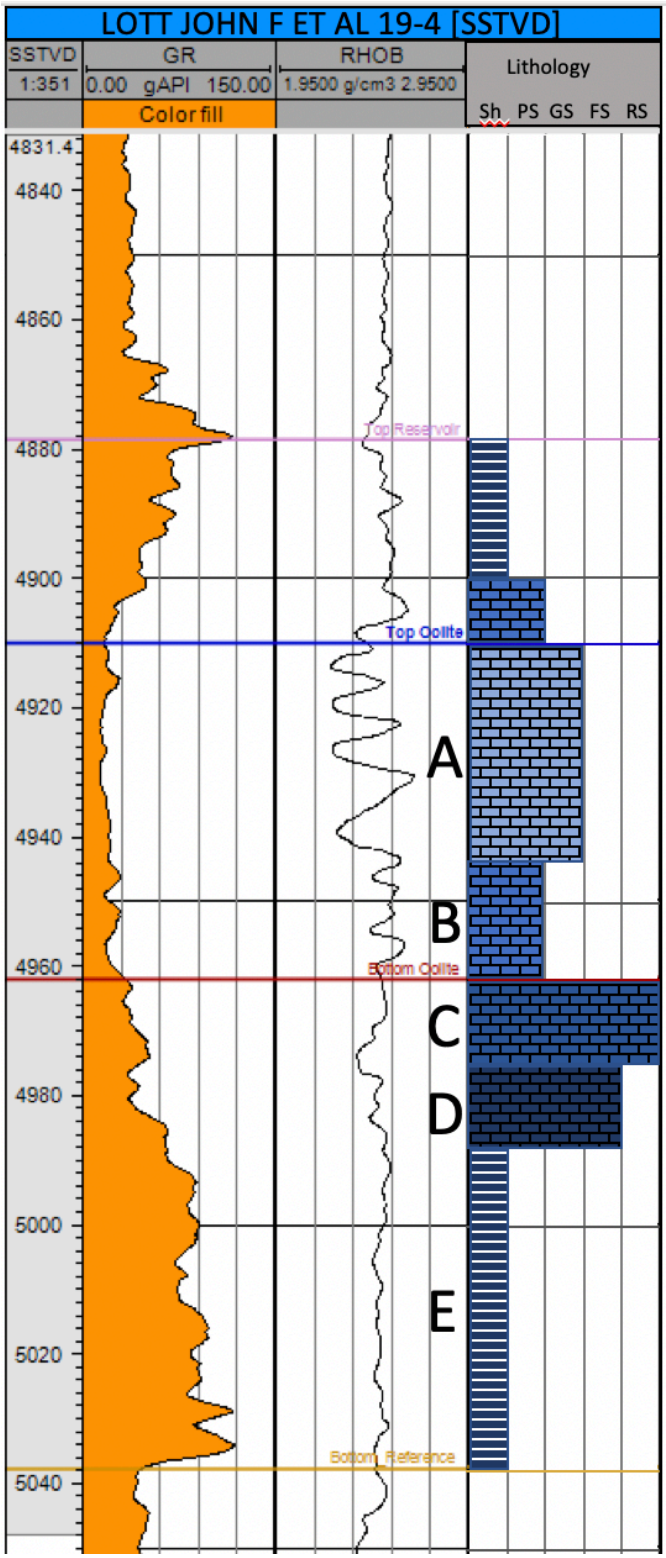

Figure 3. Type log of well 19-4. Gamma ray and bulk density tracks displayed with facies interpretation and distribution. A) Oolitic grainstone. B) Oolitic-skeletal packstone. C) Skeletal rudstone. D) Skeletal floatstone. E) Shaly siltstone.

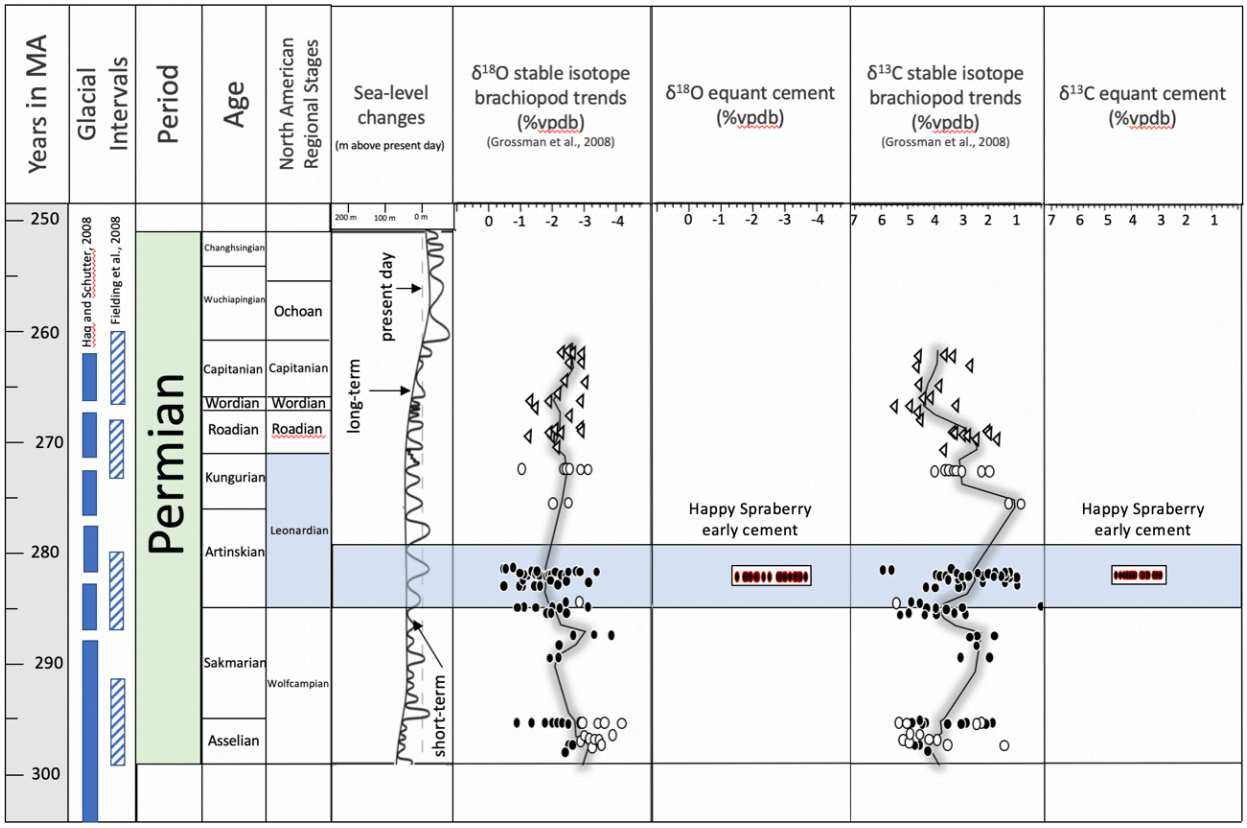

Figure 4. Stratigraphic age of Happy Spraberry succession. Age indicated as early Leonardian (blue shade). Absolute age, solid blue glacial intervals and sea level curve as proposed by Haq and Schutter, 2008. Striped glacial intervals as proposed by Fielding et al., 2008. Stable isotope trends of brachiopod shells modified from Grossman et al., 2008. Equant cement tracks represent $\delta^{13}C$ and $\delta^{18}O$ values of early equant cements analyzed from Happy Spraberry oolitic grainstone facies.

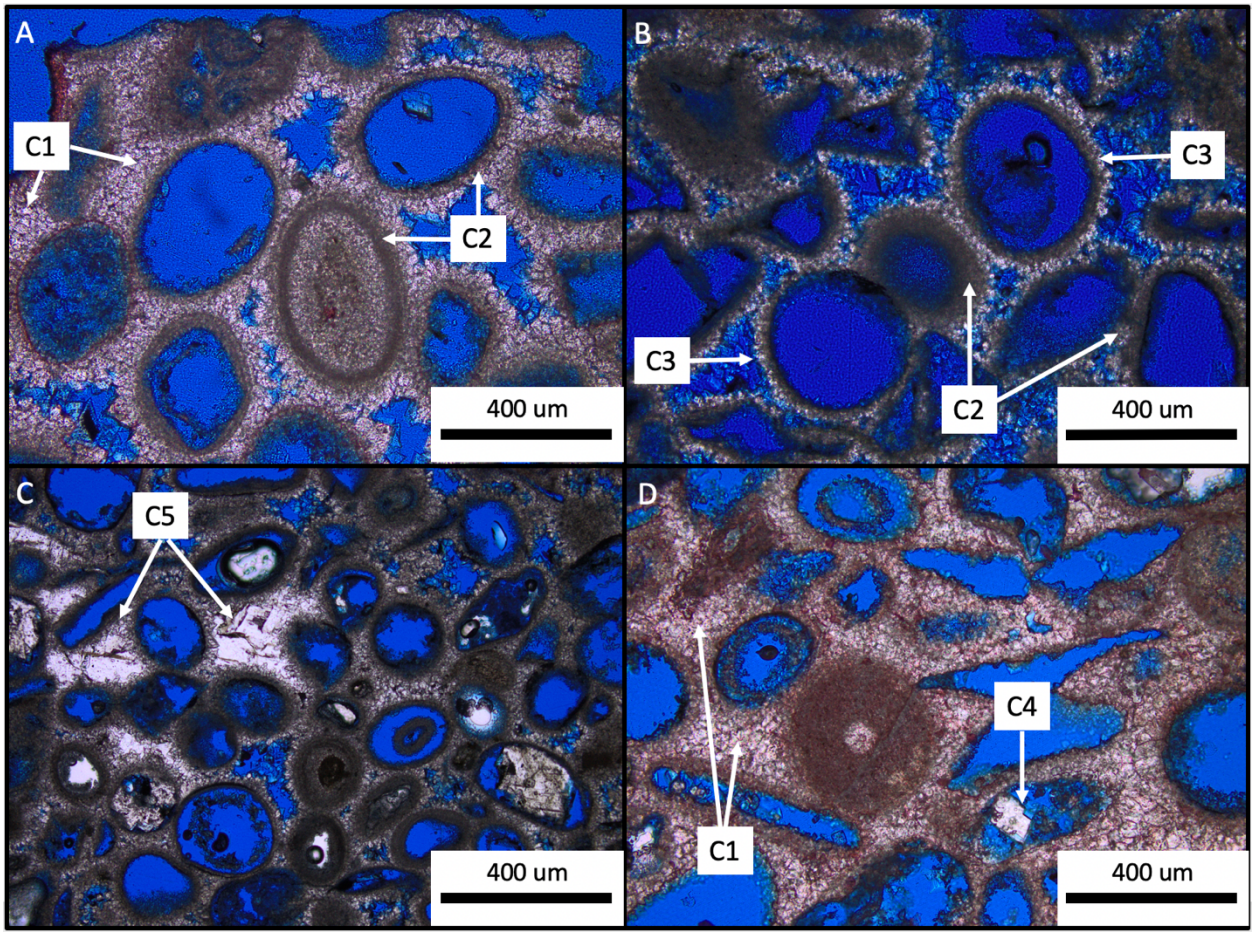

Figure 5. Thin sections showing oomoldic porosity and cement types. A) Oomolds and cemented ooid in the middle. Equant calcite cement (C1) between grains, and prominent micrite envelopes (C2) surrounding molds. B) Oomolds with isopachous calcite cement (C3). Micrite envelopes (C2) play a role in preserving porosity. C) Poikilotopic celestine (C5) in more micrite rich facies. D) Equant calcite cement (C1) between open molds and micritized ooid. Dolomite cement (C4) in oomold.

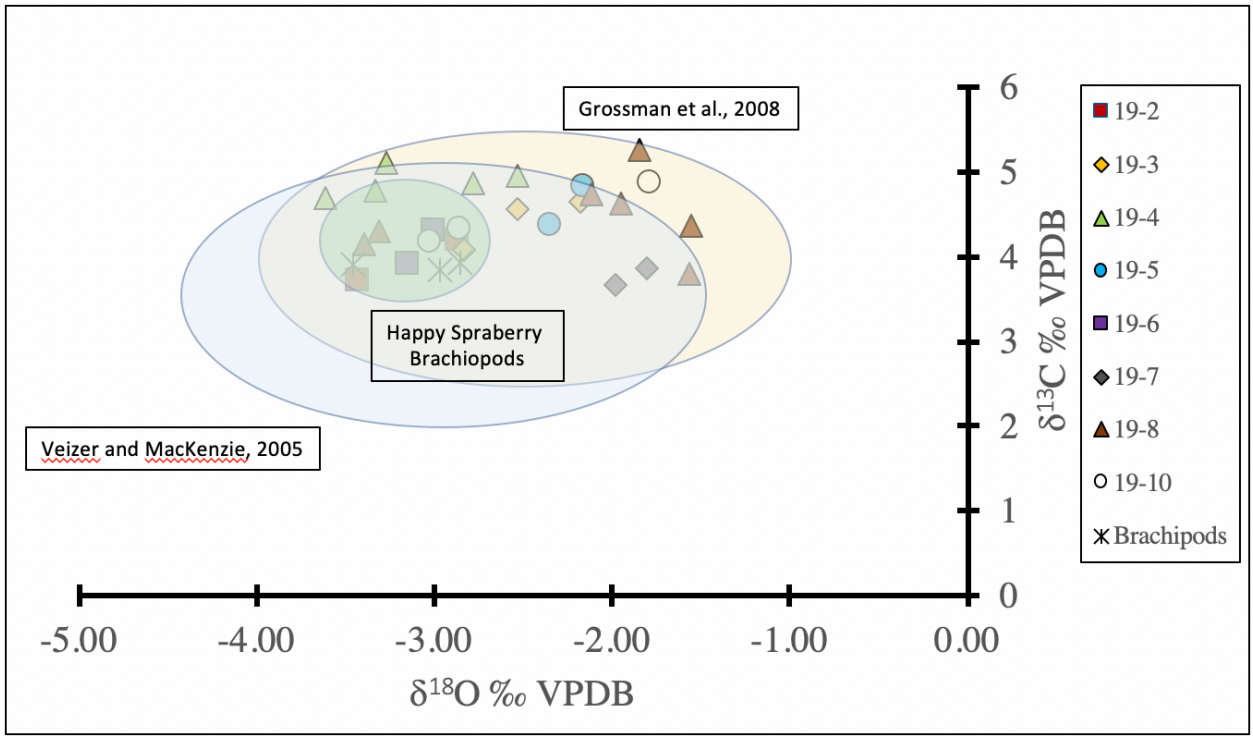

Figure 6. $\delta^{13}C$ and $\delta^{18}O$ analysis of equant cements (C1) and brachiopod shells. Shaded areas represent $\delta^{13}C$ and $\delta^{18}O$ trends for Permian marine brachiopods from Grossman et al. (2008) and Veizer and Mackenzie (2003). Green shaded area represents brachiopod $\delta^{13}C$ and $\delta^{18}O$ values from Happy Spraberry Field.

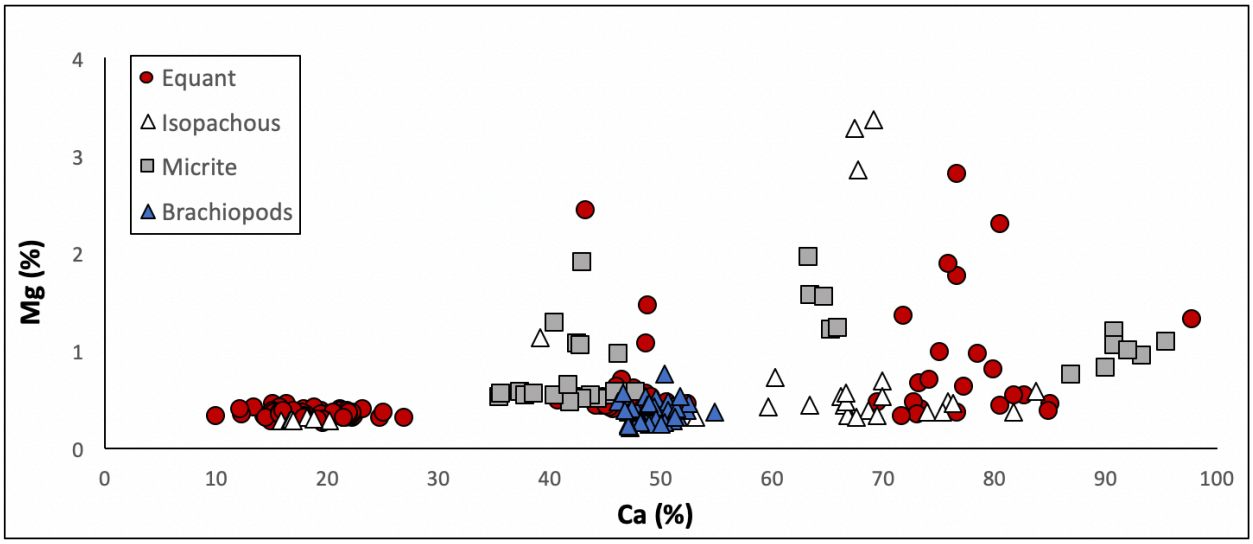

Figure 7. Ca vs Mg crossplot of cement facies and brachiopod shells. All points displayed Mg concentrations of less than 4%.

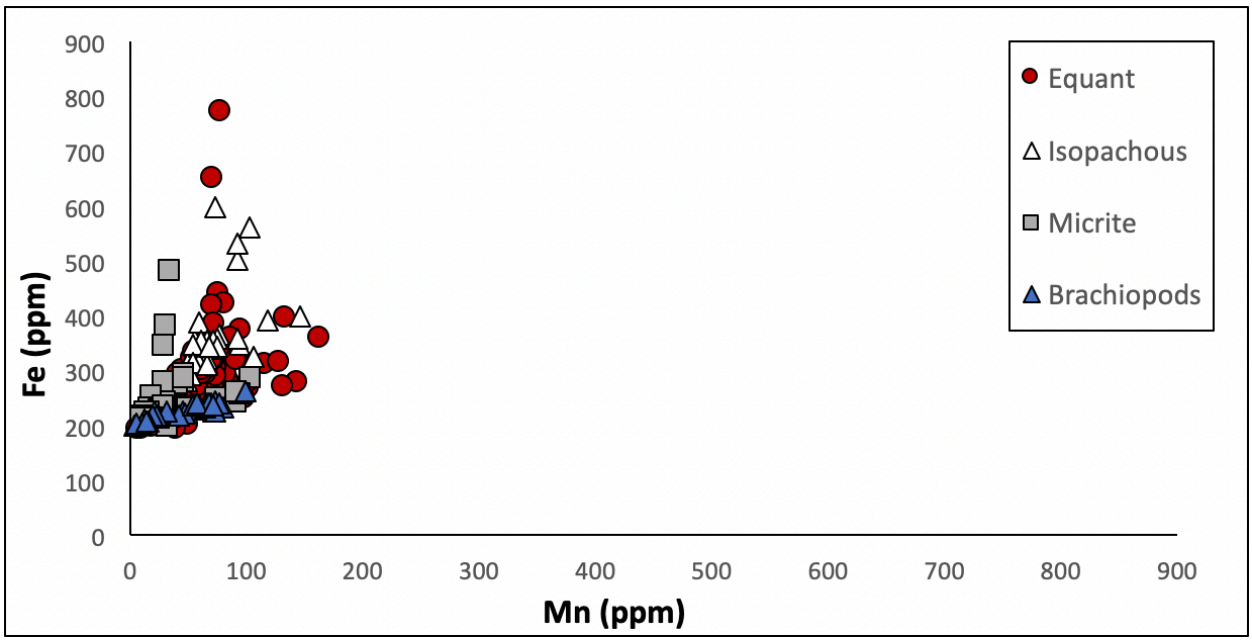

Figure 8. Mn vs Fe crossplot of cement facies and brachiopod shells. Distinctly low Mn values and relatively low Fe values are consistent throughout all sample types.

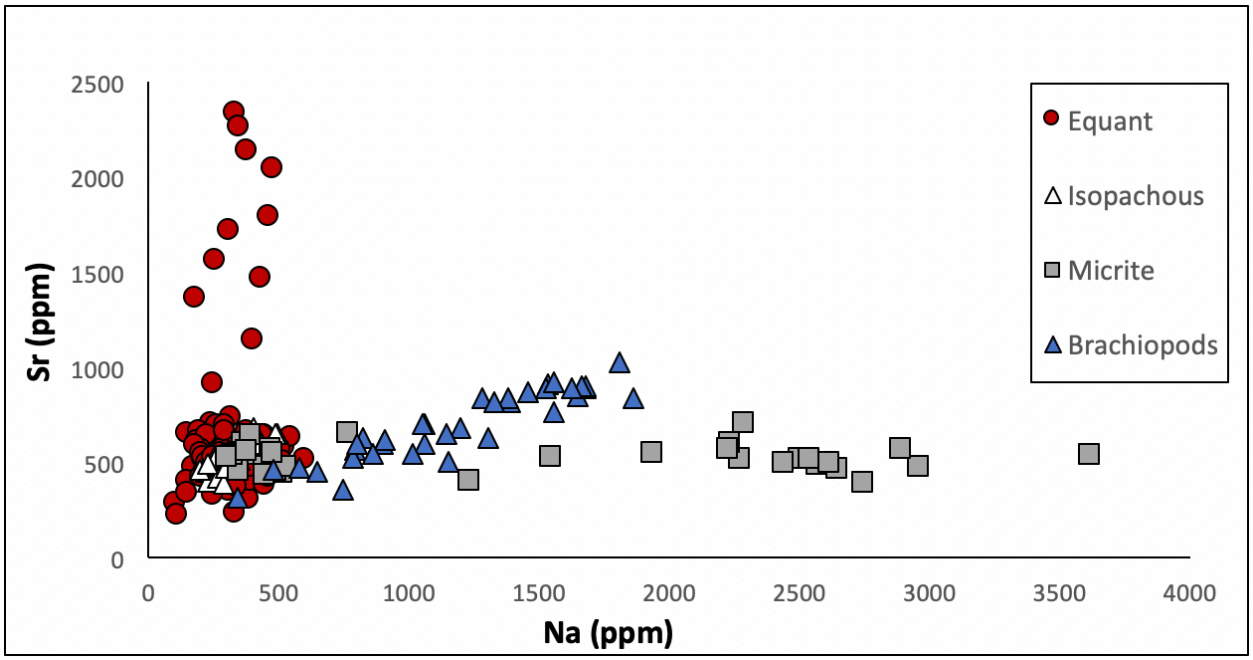

Figure 9. Na vs Sr crossplot of cement facies and brachiopod shells. Sr relatively elevated in equant cement facies due to marine water and precursor aragonite contribution. Na clearly segregated points due to preferential incorporation into calcite of biogenic origin.

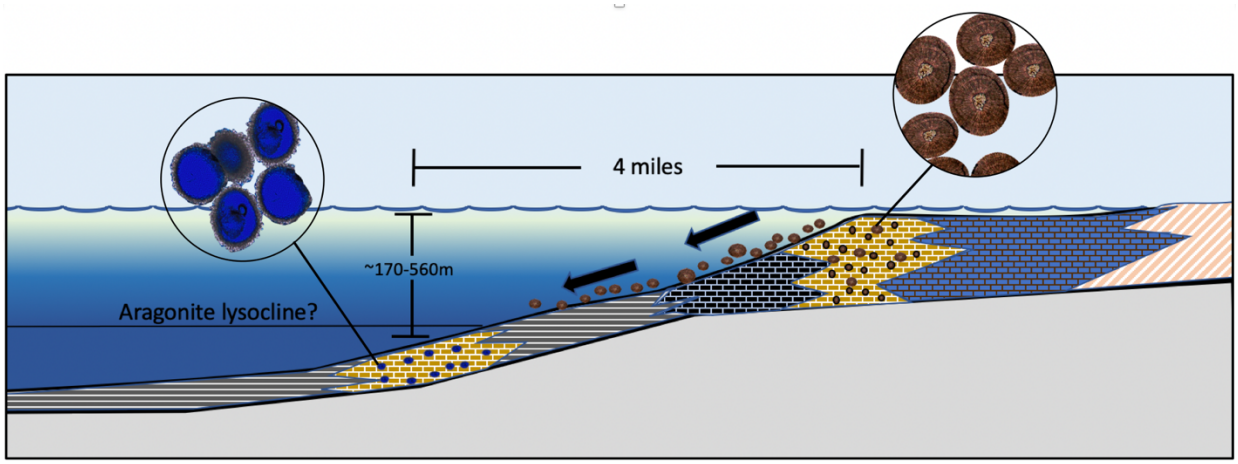

Figure 10. Conceptual model of the resedimentation process. Original genesis and deposition of aragonitic ooids in the shallow high-energy platform top and margin setting. The shedding of sediments and transportation and re-deposition in the deeper slope environment, where waters are undersaturated because of being below the aragonite lysocline. This setting promotes the dissolution of aragonitic ooids, and the creation of oomolds.

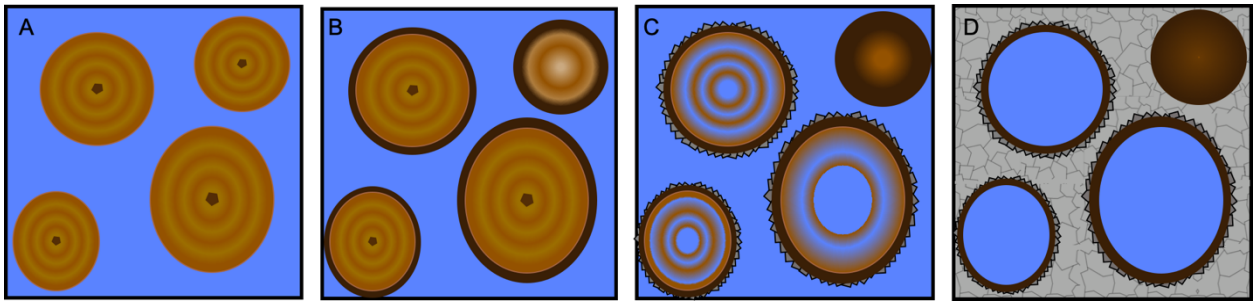

Figure 11. Schematic of diagenetic pathway of ooid grains (modified from Scholle and Ulmer-Scholle, 2003). A) Original minerology and texture of concentric aragonitic ooid grains. B) Micritization of outer layer of grains and the development of a micrite envelope by endolithic organisms in the shallow marine environment. C) Beginning of dissolution of the aragonite ooids after resedimentation into the deeper slope environment. The subsequent precipitation of isopachous rim cement. The complete micritization of an ooid grain makes it resistant to dissolution. D) The complete dissolution of ooids and the precipitation of equant calcite cement occluding primary porosity after sufficient settling time in the deeper slope environment.

APPENDIX B

TABLES

Table 1. Description of facies interpreted in Happy Spraberry Field.

Facies	Description	Interpretation
Oolitic Grainstone	The grainstone is made up of mostly ooid grains, sometimes reaching up to 75% of grain volume. Ooids are rounded to sub-rounded, and have an average diameter range of 0.2-0.4 mm. Other components include rare-common skeletal grains of crinoids, bryozoans, brachiopods, and mollusks. Most allochems are surrounded by a micritic envelope. Dissolution of originally aragonitic allochems is pronounced, making for abundant oomoldic porosity. Cements include isopachous and dominant blocky equant calcite.	Shallowest depositional environment because of the abundance of ooid grains and lack of mud. High energy environment. Oolitic shoals probably on platform top.
Oolitic-skeletal Packstone	Packstone composed of mainly ooid grains, as well as skeletal grains including crinoids, bryozoans, brachiopods, mollusks, and foraminifera. Ooid grains are rounded to sub-rounded and are rarely collapsed to compacted. Rare fine sand to silt grains. Minor lime-mud matrix. Rare dolomite cement. Micrite envelopes common across all grain types. Prominent oomoldic and moldic porosity, however some ooids are micritized. Cement types are mainly isopachous and dominant blocky equant calcite, and rare poikilotopic celestine cement.	Shallow setting with less energy than grainstone facies, due to presence of some mud as well as skeletal grains. Shallow deposition on or near platform top.
Skeletal Rudstone	Rudstone is poorly sorted, containing large >2cm lithoclasts and mudclasts, and small skeletal fragments of brachiopods, bryozoans, crinoids, mollusks, and foraminifera. It also contains rare-common ooids, peloids, and sporadic fine sand or silt grains. Lime-mud matrix common. Interparticle cements mainly blocky equant calcite cement, and secondary porosity usually occluded by micrite or equant calcite cement.	Transitional setting between high energy shoals and "quieter" slope environment, with components of both. Breakage of platform facies mixed with muddier slope facies.
Skeletal Floatstone	Floatstone is poorly sorted, containing large >2cm lithoclasts and mudclasts, and small skeletal fragments of bryozoans, and crinoids, along with rare ooids, peloids, brachiopods, mollusks, and foraminifera. Contains sporadic fine sand and silt grains. Common lime-mud matrix.	Slope facies with more prominent mud content and some contribution of upper slope facies.
Shaly Siltstone	Well sorted fine quartz silt and shale with rare skeletal grains, and common laminations.	Deeper slope setting with significant mud content. Turbidite facies.

Table 2. Bulk rock XRD analysis results for 22 samples. Calcite was the dominant component in all samples. Calcite detected was LMC with Mg concentrations ranging from 1-3%. Celestine concentrations are overestimated due to sampling bias.

Well	Depth	low-Mg Calcite	Celestine	Quartz	Dolomite
19-2	4924	97 %		3%	
19-2	4940	83%		17%	
19-3	4909	x			
19-3	4911	x			
19-3	4925	90 %		10%	
19-3	4928	93%		7%	
19-4	4913	100%			
19-4	4920	73%	27%		
19-4	4930	43%	57%		
19-4	4940	90%			10%
19-4	4958	72%	28%		
19-5	4958	100%			
19-5	4968	80%		20%	
19-6	4948	100%			
19-6	4952	100%			
19-6	4958	100%			
19-10	4935	100%			
19-11	4876	100%			
19-11	4893	90%		10%	
19-11	4899	98%		2%	
19-11	4907	84%		16%	
19-11	4913	92%		8%	

Table 3. Trace elements concentrations of cement/diagenetic facies. Analyzed facies include: 1) equant calcite cement, 2) isopachous cement, 3) unaltered brachiopod shells, 4) micritized ooids.

Well Name	Depth (tvdss)	Mg (ppm)	Fe (ppm)	Mn (ppm)	Sr (ppm)	Na (ppm)	Cement Type
19-2	4915						Equant
		4430	194.4	6.84	2037	476	
		2880	281.1	85	912	250	
		3890	266	77.7	1148	402	
		3952	194.1	11.2	2332	334	
		4360	200	50	473	175	
		3609	249.8	76.1	517	215	
		3740	269	81.8	527	321	
		3980	265.3	103.3	550	359	
		3025	292	84.1	650	152	
		3133	251.7	88.9	705	243	
		3753	242.2	67.8	674	259	
		3397	222	29.8	1795	460	
		3101	279	143.5	578	216	
		2909	246.7	99.9	284.8	105	
		3900	198.6	26.5	1557	257	
		3418	255.8	70.5	660	197	
		2980	277	103.5	401	149	
		3290	245	63.3	343	148	
		3671	195.3	18.73	2136	377	
		3111	274.1	56.2	1717	313	
		2921	319	72.3	1472	430	
		3037	263.5	39.4	1360	179	
		3147	260	65.2	446	435	
		4095	202	13.9	2261	349	
		2844	271.5	132	221.1	113	
		3070	650	71.5	610	186	
		3058	270.4	55.4	731	317	
		3399	252.3	77.5	499	294	
		2820	440	76.1	612	223	
		3026	266.8	66.3	691	267	
		3544	283.5	59.4	596	304	
		3309	305	74.2	557	250	
19-4	4913						Equant
		3370	285	56	464	226	
		3375	299	46	690	294	
		3343	305	72	639	452	
		3457	260	52	511	315	
		3570	358	86	526	330	
		2524	257	43	542	233	
		3490	281	54	508	316	
		3400	258	42	528	327	
		3322	296	63	491	269	
		3479	270	49	569	289	
		2780	256	40	640	228	
		2989	292	44	512	251	
		3584	275	53	661	294	
		3373	272	74	447	258	
		3484	246	47	525	419	
		3013	250	53	426	207	
		3547	277	63	584	526	

Table 3. (continued)

Well Name	Depth (tvdss)	Mg (ppm)	Fe (ppm)	Mn (ppm)	Sr (ppm)	Na (ppm)	Cement Type
19-4 (continued)	4913						Equant
		3200	321	54	546	282	
		3155	280	70	512	235	
		4080	296	66	499	310	
		3386	291	72	544	350	
		2611	271	55	523	225	
		2958	313	71	466	280	
		2813	302	60	568	206	
		3750	330	78	410	239	
		3026	290	76	458	223	
		2759	300	60	586	181	
		3520	281	60	511	326	
		2930	264	46	470	273	
		3330	254	35	564	367	
		3740	281	54	537	353	
		3950	243	37	504	273	
19-4	4920						Equant
		3240	348	87.4	582	420	
		3069	373	96	522	301	
		3254	358	164	354	308	
		3018	300.4	51.4	615	423	
		3461	312.3	117	234.1	336	
		3165	315	128	373	359	
		3700	324	93.3	383	398	
		3160	396	133.5	471	234	
19-4	4920						Isopachous
		3100	58.6	58.6	650	496	
		2746	118.1	118.1	465	227	
		2758	47.5	47.5	530	261	
		2879	93.7	93.7	449	216	
		2826	105.4	105.4	400	228	
		2918	52.9	52.9	628	412	
		2807	66.5	66.5	683	406	
		2997	77.3	77.3	649	486	
19-11	4893						Isopachous
		6970	75	75	595	369	
		3780	59	59	574.3	327	
		3760	68.9	68.9	578.5	410	
		3910	67.4	67.4	531.8	267.1	
		4440	66.8	66.8	487.5	244.5	
		4750	52.4	52.4	524	299	
		32800	103.2	103.2	417.7	262.7	
		5340	61.5	61.5	516.1	248.3	
		3677	33.5	33.5	539.4	288	
		33700	92.5	92.5	391.1	285.6	
		28600	92.2	92.2	516	346	
		5350	66.7	66.7	497	258	
		11400	73.5	73.5	488		
		3346	48.5	48.5	530.6	247.3	
		4600	146.2	146.2	513	271	
		4670	59	59	464	198.9	

Table 3. (continued)

Well Name	Depth (tvdss)	Mg (ppm)	Fe (ppm)	Mn (ppm)	Sr (ppm)	Na (ppm)	Cement Type
19-11 (continued)	4893						Isopachous
		5580	92.8	92.8	469.9	306	
		5890	71.8	71.8	531.3	259.8	
		3117	60.9	60.9	589	348	
		4390	75.6	75.6	601.7	430	
		7230	54.7	54.7	600	358	
		3229	54	54	491.7	226.1	
		4150	65.6	65.6	472	296	
		3412	67.7	67.7	560	307	
19-11	4893						Micrite
		7350	225.9	26.7	399	1237	
		8040	234.5	29.1	522	1547	
		11780	213.2	21.5	545	1938	
		10390	222.9	17	513	2276	
		9430	222.5	14.83	603	2234	
		10860	217	12.34	570	2232	
		9910	211.1	10.46	481	2570	
		15660	241.4	92.2	496	2620	
		19500	287	104.5	518	2500	
		12050	248.8	75	494	2440	
		15350	257.5	95.4	569	2890	
		12160	259	92.8	519	2540	
19-11	4893						Equant
		4350	283.3	43.4	611	391	
		5340	315.8	62	542.1	376	
		17600	369	67.2	480.2	385	
		9500	285.3	49.8	536	424	
		4240	270.6	58.5	558	360	
		28000	770	77.8	479	398	
		3711	291.6	42.7	572	508	
		5260	319.1	71.4	458.5	222	
		7900	354	71.8	509	310	
		22800	422	82.6	506	516	
		3950	291	65.7	490	257	
		13070	375	66.9	427	467	
		4560	284.5	44.6	546.3	205	
		3420	302.9	56.8	529	214	
		6120	318.3	91.8	455.9	259	
		18700	419	70.7	440	240	
		3490	299.8	66	529.5	256	
		6600	307.7	64.6	497	224	
		4550	292.9	62.3	506.5	297	
		3134	300.1	63	509.8	264	
		6860	333	55.2	599	391	
		13500	384	72.8	479	250	
		9720	322.3	60.2	526	252	
19-11	4899						Micrite
		5520	208	27.84	540	373.9	
		5350	197.9	32.53	489.3	469	
		4900	229.8	25.9	597	364	
		5610	213	26.3	537.1	471	

Table 3. (continued)

Well Name	Depth (tvdss)	Mg (ppm)	Fe (ppm)	Mn (ppm)	Sr (ppm)	Na (ppm)	Cement Type
19-11 (continued)	4899						Micrite
		5587	211.5	23.39	552.8	351.9	
		5580	217.4	26.21	568.2	473	
		4945	278	47.5	446.3	517	
		5126	291	47	451.3	491	
		4930	271.3	41.6	473.2	445	
		5271	273.4	42.7	472.8	534	
		5013	287	47.19	430.6	452	
		4586	229.2	50.6	457	348.8	
		5560	479	35.3	547.3	478	
		5170	277	29.36	542	322.7	
		5420	239.3	31.14	641	392.9	
		5219	344	30.19	536.3	326.5	
		5280	382	31.9	532	304.2	
		5383	277	29.67	560	378	
		6300	221	24.9	650	771	
		18900	251	20.14	479	2960	
		10650	218.7	20.77	702	2290	
		9460	226.4	21.66	468	2650	
		10480	229.3	17.27	395	2750	
		12700	220	18.3	535	3620	
19-11	4899						Equant
		14600	318	73.8	485.1	306	
		4500	228.6	31.51	567	415	
		4400	249.6	48.2	561	424	
		4990	213.6	27.56	444.1	524	
		6250	191.8	40.9	306	388	
		5010	228.5	37.1	533	422	
		6050	254.5	57.9	560	481	
		6890	196.6	33.7	328.9	252	
		5400	214.5	40.8	398.4	396	
		5030	209	31.8	384	445	
		24200	285	43.9	476	348	
		10670	266	51.4	484	259	
		4294	238.6	27	489	352	
		4217	267.2	48	534.6	305	
		3800	260.6	32.9	527	385	
		4247	224.1	39.9	403.1	264	
		4620	228.9	34.04	418	342	
		4233	212.1	29.9	413.6	289	
		4110	267.5	43.4	548.2	394	
		4240	272.3	40.1	665	377	
		5060	269.1	36.2	632	546	
		4743	210.6	40.4	366.6	340	
		5140	228.2	18.34	643	440	
		6140	220.8	14.56	520	604	

Table 3. (continued)

Well Name	Depth (tvdss)	Mg (ppm)	Fe (ppm)	Mn (ppm)	Sr (ppm)	Na (ppm)	Cement Type
19-10	4931						Brachiopod
		3173	234.1	79.6	604	1056	
		2913	217.1	24.1	918	1533	
		2612	202.4	3.8	1028	1805	
		3175	226.2	45.3	700	1061	
		4450	229.8	61	603	903	
		3627	217.5	24.2	894	1526	
		3864	222.7	30.7	823	1392	
		3910	235.4	66.7	449	645	
		4610	262.5	98.8	628	1304	
		5100	228.1	72.1	471	575	
		3768	224.8	72.8	357.5	746	
		4790	223.3	47	460.2	482	
		4810	245.8	72.5	552	1013	
		4730	234.5	65.3	511	1150	
		7550	219.6	41.4	836	1861	
		3820	237.6	69.5	630	820	
		5630	236	58.5	621	909	
		5290	236.6	65	568	796	
		4010	236.9	68.3	530	781	
		4170	242.1	76.9	597	801	
		4460	241.6	66	686	1197	
		4610	237.1	53.7	764	1554	
		4037	242.1	70.3	704	1055	
		5210	242.5	67.3	544	861	
		2492	210.7	11.92	836	1282	
		2678	205.5	10.56	835	1377	
		2788	225.3	21.4	821	1328	
		2925	227.5	31.4	855	1648	
		2620	217.3	22	896	1680	
		2531	202.8	9.86	904	1679	
		3145	240.1	57.3	657	1145	
		2625	218.1	19.2	908	1663	
		2159	209	15.11	922	1557	
		2280	203.4	5.04	869	1459	
		2512	209.6	14.2	897	1627	
		3864	236.7	71	320	345	